Using Native Chemical Ligation for Site-specific Synthesis of Hetero- bis-lanthanide Peptide Conjugates: Application to Ratiometric Visible or Near-infrared Detection of Zn 2+

Céline Cepeda, Laurent Raibaut, Guillaume Fremy, Svetlana Eliseeva, Anthony Romieu, Jacques Pécaut, Didier Boturyn, Stéphane Petoud, Olivier Sénèque

Using Native Chemical Ligation for Site-specific Synthesis of Hetero-bis-lanthanide Peptide Conjugates: Application to Ratiometric Visible or Near-infrared Detection of Zn^{2+}

Céline Cepeda,[ab] Laurent Raibaut,[a] Guillaume Fremy,[ab] Svetlana V. Eliseeva,[c] Anthony Romieu,[d] Jacques Pécaut,[e] Didier Boturyn,[b] Stéphane Petoud,*[c] and Olivier Sénèque*[a]

[a] Univ. Grenoble Alpes, CNRS, CEA, IRIG, LCBM (UMR 5249), F-38000 Grenoble, France.

[b] Univ. Grenoble Alpes, CNRS, DCM (UMR 5250) F-38000 Grenoble, France.

[c] Centre de Biophysique Moléculaire, UPR CNRS 4301, Université d'Orléans, rue Charles Sadron, F-45071 Orléans, France.

[d] ICMUB, UMR 6302, CNRS, Univ. Bourgogne Franche-Comté, 9 Avenue Alain Savary, 21000 Dijon, France.

[e] Univ. Grenoble Alpes, CEA, CNRS, IRIG, SyMMES, F-38000 Grenoble, France.

Email: *olivier.seneque@cea.fr* and *stephane.petoud@inserm.fr*

Abstract

The interest for ratiometric luminescent probes that detect and quantify a specific analyte is growing. Due to their special luminescence properties, lanthanide(III) cations offer attractive opportunities for the design of dual-color ratiometric probes. Here, we describe the design principle of hetero-bis-lanthanide peptide conjugates using native chemical ligation for a perfect control of the localization of each lanthanide cation within the molecule. Two zinc-responsive probes, **r-LZF1**$^{\mathbf{Tb|Cs124|Eu}}$ and **r-LZF1**$^{\mathbf{Eu|Cs124|Tb}}$ are described on the basis of a zinc finger peptide and two DOTA complexes of terbium and europium. Both display dual-color ratiometric emission responding to the presence of Zn^{2+}. Using a screening approach, anthracene was identified for the sensitization of the luminescence of two near infrared-emitting lanthanides, Yb^{3+} and Nd^{3+}. Thus, two novel zinc-responsive hetero-bis-lanthanide probes, **r-LZF3**$^{\mathbf{Yb|Anthra|Nd}}$ and **r-LZF3**$^{\mathbf{Nd|Anthra|Yb}}$ were assembled, the former offering a neat ratiometric response to Zn^{2+} with emission in the near-infrared around 1000 nm, which is unprecedented.

Introduction

Fluorescence – or more generally luminescence – is a highly sensitive, inexpensive and easy-to-use analytical technique that finds a large scope of applications in various scientific and medical fields, including analytical chemistry, biological research,[1] medical diagnosis[2] and image-guided surgery.[3,4] Responsive luminescent probes capable of detecting a specific molecular species in a complex medium are in high demand today and find many applications, for instance, in biology to obtain a better knowledge of molecular processes at play in living organisms[5–10] or to detect relevant disease biomarkers.[11] Luminescent probes most often offer an intensity-based response: the interaction (reversible binding or chemical reaction) with the analyte turns the emission ON or OFF with a uniform evolution over the whole emission spectrum. Such probes are the easiest to design for a chemist and quantification of the analyte is possible provided that the concentration of the probe is known. However, in a complex biological medium such as a living cell or whole organism, the spreading of the probe may not be uniform and its concentration may vary depending on its location, thereby precluding quantification of the analyte. It is possible to overcome this issue by designing ratiometric probes that feature dual-wavelength excitation or emission. The ratio of intensities observed at two different wavelengths (excitation or emission) provides a reliable signal read-out that is independent of the probe concentration. Most common ratiometric probes display a dual-wavelength emission due to a spectral shift caused by an interaction with the analyte.[12] For such probes, the emission ratio measured at two wavelengths is directly related to the analyte concentration.

Complexes of trivalent lanthanide cations (Ln^{3+}) have fantastic luminescent properties. They offer an attractive alternative to the classical organic dyes, especially for biological application.[13–17] They possess (i) atom-like narrow emission bands at fixed wavelength that are independent of the experimental conditions and characteristic of the nature of the Ln^{3+}, (ii) a large energy difference between the excitation and emission wavelengths, (iii) long luminescence lifetimes (micro to millisecond range) allowing suppression of background fluorescence by time-resolved detection and (iv) an excellent photostability. Since most 4*f*-4*f* transitions are forbidden by Laporte rules,[18] an efficient strategy for the sensitization of lanthanide cations to generate their luminescence is based on the excitation of a proximal highly-absorbing organic chromophores (antenna) that can transfer the resulting energy to the Ln^{3+} in order to populate its emissive excited state. This process has been termed the "*antenna effect*". Several responsive lanthanide-based luminescent probes have been described to date but only few of them are ratiometric.[14,17] Actually, lanthanides offer two options to elaborate ratiometric probes. First, the relative intensity of each Ln^{3+} emission band and the shape of these bands depend on the Ln^{3+} coordination environment. Hence, ratiometric responsive sensing can be obtained in the case of coordinatively unsaturated luminescent Ln^{3+} complexes that allow the analyte to replace one or two coordinated water molecules in the Ln^{3+} coordination sphere.[19–23] This alters the geometry and symmetry around the Ln^{3+} affecting the intensity ratios between the different f-f transitions and their Stark splitting. In this respect, Eu^{3+} is the most interesting Ln^{3+} due to the high sensitivity of its emission bands to changes in coordination environment. Emission of other Ln^{3+} like Tb^{3+}, for example, is less affected and changes are subtler.[21] The second approach for the design of Ln-based ratiometric probes takes advantage of their narrow emission bands with fixed emission wavelengths and uses two different Ln^{3+} whose emissions vary in different ways upon interaction of the probe with the analyte. The simplest approach in this respect is to exploit a pair of responsive and non-responsive Ln^{3+} complexes with distinct emission profiles. In such a mix, the non-responsive complex serves as a reference for the calibration of the responsive probe. The Ln^{3+} chelating ligands may be different for the two complexes[24] but, nevertheless, for biological imaging applications in living cells, it is recommended to use the same ligand in order to favour the same biodistribution of the responsive and non-responsive complexes in order to allow an accurate calibration .[25–29] This approach requires a common

antenna that is able to sensitize both Ln^{3+}. To date, the Tb^{3+}/Eu^{3+} pair has been widely used not only because of the availability of numerous antennas that can sensitize both cations but also because they exhibit easily detectable visible emission with long luminescence lifetimes within the millisecond range compared to microseconds for other Ln^{3+}. Tb^{3+} and Eu^{3+} emission spectra overlap in the 560-670 nm spectral range but distinct and specific emission bands can be monitored at 490 and 545 nm for Tb^{3+} and 700 nm for Eu^{3+} (Figure 1). The proportion of Tb^{3+} and Eu^{3+} complexes in the global mixture can be adjusted to compensate for the differences in sensitization and emission efficiencies in order to provide emissions intensities in the same dynamic range for both complexes.

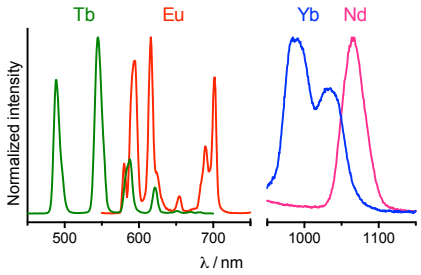

Figure 1: Examples of emission spectra of Tb^{3+}, Eu^{3+}, Yb^{3+} and Nd^{3+} with DOTA-monoamide ligands obtained from compounds **LZF1**$^{Cs124|Tb}$, **LZF1**$^{Cs124|Eu}$ and **LZF1**$^{NBD|Nd}$ for Tb^{3+}, Eu^{3+} and Nd^{3+},[30] respectively, and compound LZF3$^{Anthra|Yb}$ for Yb^{3+} (this work).

Nevertheless, even if based on the same ligand, the use of a mix of two distinct Ln^{3+} complexes do not fully ensure that the ratio of the two complexes is kept constant in cells as subtle changes in structure can affect biodistribution of molecules (possible discrepancy might arise from difference in Ln^{3+} ionic radius or hydration). Therefore, designing ratiometric probes with two distinct Ln^{3+} within the same molecules appears an interesting strategy to overcome this problem. For such a strategy we can envisage either a single antenna adapted both Ln^{3+} or a pair of antennas, each sensitizing one of the Ln^{3+}. The main challenges in this strategy is to selectively introduce each of the two Ln^{3+} in a specific site of the molecule and to avoid scrambling. Such regiospecific hetero-bis-lanthanide complexes remain scarce. An example of hetero-bis-lanthanide complex with site-specific metalation was reported by Sames et al. with a DOTA/DTPA bis-chelate (DOTA = 1,4,7,10-tetraaza-cyclododecane-1,4,7,10-tetraacetic acid, DTPA = diethylene-triaminepentaacetic acid).[31] The kinetic inertness of the DOTA macrocycle compared to DTPA was exploited to specifically metalate this molecule with a Tb^{3+} and Eu^{3+} pair at chosen chelating sites (in this case, Tb^{3+} in DOTA and Eu^{3+} in DTPA). The emission spectrum of this molecule is dependent on the solvent polarity. Faulkner et al. used the four-component Ugi reaction to covalently assemble two DOTA-Tb^{3+} and DOTA-Eu^{3+} complexes and a naphthalene antenna thereby providing an O_2-responsive ratiometric probe featuring a Tb^{3+}/Eu^{3+} pair at controlled positions.[32] Interestingly, the Tb/Eu probe and the inverted Eu/Tb counterpart do not behave the same toward O_2. In this article, we describe a novel strategy relying on native chemical ligation[33,34] (NCL) to assemble hetero-bis-lanthanide ratiometric responsive probes based on a peptide scaffold. Indeed, by assembling two peptide segments, each containing a distinct DOTA-Ln^{3+} complex, we were able to get two ratiometric probes that respond to Zn^{2+}, a cation of interest in living systems.[30,35–40] The first one features the classical visible-emitting Tb^{3+}/Eu^{3+} pair while the second one features a NIR-emitting Yb^{3+}/Nd^{3+} pair, which is unprecedented.

Results and discussion

Design of hetero-bis-lanthanide peptide Zn^{2+}-responsive probes

During the past years, we have described several responsive luminescent probes combining luminescent lanthanides, for their emission properties, and peptides, for their highly specific recognition properties.[30,40–43] Especially, we have shown that a classical ββα zinc finger peptide with an appended DOTA-Ln^{3+} complex and a suitable antenna can operate as a turn-ON intensiometric luminescent probe for the detection of Zn^{2+}.[30] Zinc fingers are small protein domains that bind a Zn^{2+} ion thanks to a set of four cysteine and histidine residues. Among them, classical ββα zinc fingers possess a (Tyr/Phe)-Xaa-Cys-$Xaa_{2/4}$-Cys-Xaa_3-Phe-Xaa_5-Leu-Xaa_2-His-Xaa_3-His consensus sequence, where Xaa can be any amino acid. The peptide is folded into a double-stranded β-sheet and an α-helix when bound to zinc but it is unfolded in its Zn^{2+}-free form. To take advantage of this conformational change, we have grafted a DOTA-Ln^{3+} complex and a sensitizing antenna onto the peptide in remote positions in the sequence that come in close proximity when the peptide folds upon Zn^{2+}-binding. Hence, the efficiency of the antenna effect increases upon Zn^{2+} binding, thereby increasing the Ln^{3+} emission intensity. Our system is quite versatile by its design, allowing to change the nature of the Ln^{3+} and the corresponding antenna to control both the emission and excitation wavelengths. The first family of luminescent zinc finger-based probes, named **LZF1$^{\text{antenna|Ln}}$**, encompass visible-emitting probes were obtained with Tb^{3+} or Eu^{3+} as a lanthanide and a NIR-emitting probe was obtained with Nd^{3+}.[30,40] Depending on the **LZF1$^{\text{antenna|Ln}}$** probe, the Ln^{3+} emission intensity is increased 8 to 30 times in response to Zn^{2+}. In order to improve the properties of these probes, we thought to design ratiometric probes instead of intensiometric ones by adding a second lanthanide emitter. Our hypothesis was to keep the previous design with antenna and Ln^{3+} complex (Ln1 in Figure 2A) at the same positions in the sequence and to choose a second Ln^{3+} (Ln2 in Figure 2A) that can be sensitized by the same antenna. We decided to graft the second Ln^{3+} complex (Ln2) at the N-terminus, in close proximity to the antenna. In this case, the distance between the antenna and Ln2 is short enough to ensure a proper sensitization and to ensure that it is unaffected by Zn^{2+}-induced folding of the probe. Therefore, we were expecting the emission of Ln1 to increase upon Zn^{2+} binding but the emission of Ln2 to be almost constant for self-calibration purpose. Our first hetero-bis-lanthanide probe was based on the Tb^{3+}/Eu^{3+} pair and an amide derivative of Carbostyril 124 (Cs124, 7-amino-4-methyl-2(1*H*)-quinolinone) was selected as an antenna because it is known to readily sensitize both of these Ln^{3+}.[30,44]

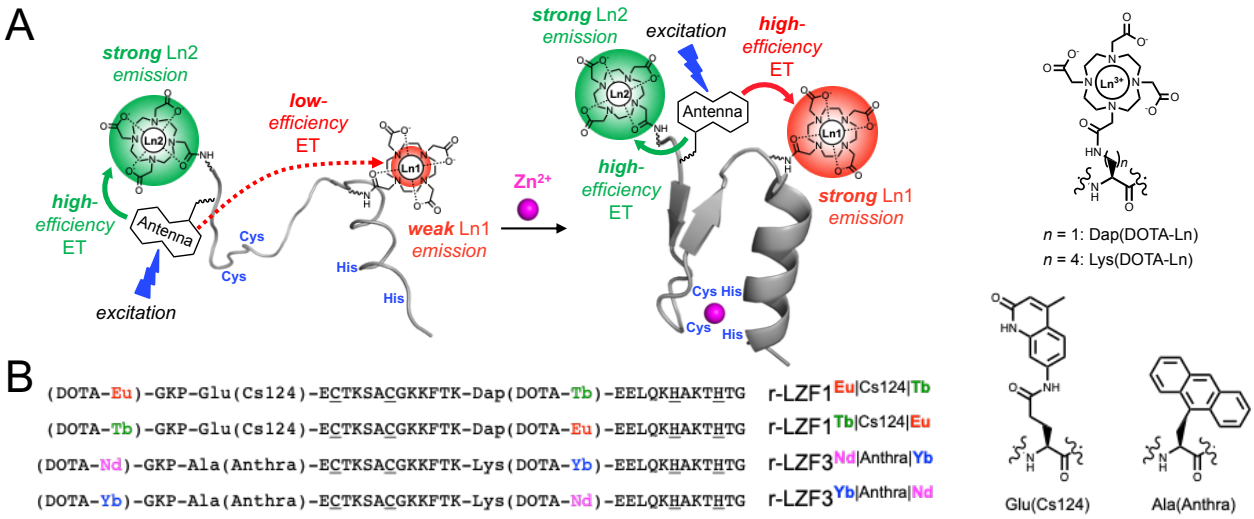

Figure 2: (A) Principle of dual-color ratiometric Zn^{2+}-sensing by r-**LZF** peptides (ET = energy transfer). (B) Amino acid sequences of **r-LZF** peptide probes with Zn^{2+}-binding cysteines and histidines underlined.

Design of hetero-bis-lanthanide peptide Zn^{2+}-responsive probes

As mentioned in the introduction, the main issue in the synthesis of hetero-bis-lanthanide compounds lies in the accurate control of the location of the two Ln^{3+} within the molecule. It would have seemed possible to graft the DOTA-Ln^{3+} complexes by chemoselective (click) reactions such as copper-catalysed alkyne-azide cycloaddition (CuAAC) or thiol-maleimide coupling. However, CuAAC is not suitable for peptides with many cysteine or histidine residues such as zinc fingers because of their high affinity for copper(I). Thiol-maleimide ligation would be difficult to control because of the presence of Zn-binding cysteines in the peptide. Zinc finger peptide comprises several cysteines that can be used to chemically synthetize the zinc finger protein by NCL.[45,46] Compared to other chemoselective ligations, NCL allows the assembly of two peptide segments by establishing a native amide bound between them, ensuring that neither the nature of the final zinc finger protein nor its folding properties are impaired. Additionally, this strategy allows using in both segments the thermodynamically and kinetically DOTA-Ln^{3+} complex, which is an asset in view of acidic HPLC conditions required for the purification of peptides. Thus, our strategy was to prepare two peptide segments, each of them comprising a DOTA-Ln^{3+} complex, but with a distinct Ln^{3+}, and to assemble them by NCL[33,34] to get a peptide with Tb^{3+} and Eu^{3+} at chosen pre-defined positions (Figure 3). The amidated C-terminal cysteinyl segment contains a DOTA-Ln^{3+} complex whereas the N-terminal segment with a SEA latent thioester (SEA = *bis*(2-sulfanylethyl)amido) contains the amidated Cs124 antenna and the second DOTA-Ln^{3+}. The C-terminal segment was synthesized on Rink Amide resin using an Alloc-protected diaminopropionic acid (Dap) residue, which can be selectively deprotected by Pd^0, to selectively incorporate the DOTA ligand using DOTA-*tris*(*t*Bu)ester as a reagent (see Supporting Information for details of the synthesis). After resin cleavage and removal of protecting groups, this segment was metalated with either Tb^{3+} or Eu^{3+}. The N-terminal segment was synthesized on SEA-PS resin using the Fmoc-Glu(Cs124)-OH building block to incorporate the antenna during peptide elongation and the N-terminus was capped by coupling DOTA-*tris*(*t*Bu)ester. After resin cleavage and removal of protecting groups, this segment was metalated with either Tb^{3+} or Eu^{3+} as well.

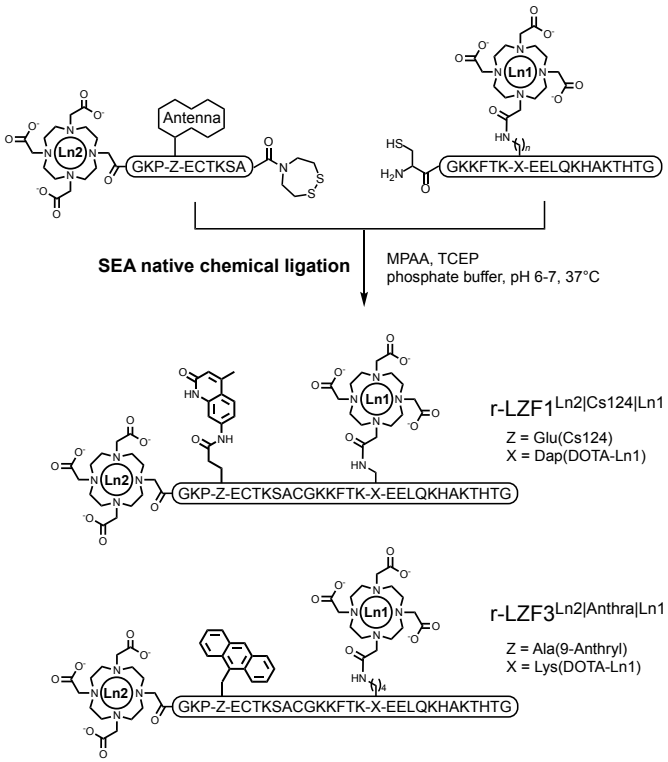

Figure 3: Synthesis of **r-LZF** probes by native chemical ligation.

As a next step, in order to check that the scrambling of Ln^{3+} cannot occur, the Tb-loaded N-terminal and Eu-loaded C-terminal segments were mixed in an ammonium acetate buffer at neutral pH. After 3 days on stirring, no trace of Eu-loaded N-terminal segment or Tb-loaded C-terminal segment could be detected by ESI-MS (electrospray ionization mass spectrometry). This indicates that no exchange of Ln^{3+} occurs between the two DOTA units (Figure S8 of Supporting Information). Thus, the Tb-loaded N-terminal and Eu-loaded C-terminal segments were readily assembled by SEA ligation conducted in phosphate buffer in the presence of MPAA (4-mercaptophenylacetic acid) and TCEP (*tris*(carboxyethyl)-phosphine) to trigger the NCL. This synthesis afforded peptide **r-LZF1$^{\mathbf{Tb|Cs124|Eu}}$** (Figure 2B). Similarly, because the respective positions of Tb^{3+} and Eu^{3+} might be important, peptide **r-LZF1$^{\mathbf{Eu|Cs124|Tb}}$** (Figure 2B), with inverted Tb^{3+} and Eu^{3+} sites, was obtained from the Eu-loaded N-terminal and Tb-loaded C-terminal segments. Both peptides were obtained as pure products and were identified by ESI-MS analysis (Figure S7 of Supporting Information).

Characterization of ratiometric probes emitting in the visible

The luminescence properties of **r-LZF1$^{\mathbf{Eu|Cs124|Tb}}$** and **r-LZF1$^{\mathbf{Tb|Cs124|Eu}}$** were investigated in HEPES buffer at pH 7.5. When the antenna is excited at 330 nm, the characteristic emissions of the antenna (Figures S9 and S10 of Supporting Information) as well as Tb^{3+} and Eu^{3+} are observed for both peptides. Excitation spectra of Tb^{3+} (λ_{em} = 545 nm) and Eu^{3+} (λ_{em} = 700 nm) confirm that both lanthanides are sensitized by the amide derivative of Cs124. The normalized time-resolved emission spectra (100 µs delay) of the Zn-free peptides are displayed in Figure 4A. In both cases, the terbium emission dominates the europium one, which is not surprising since this antenna is known to sensitize Tb^{3+} more efficiently than Eu^{3+}.[25] Comparatively, the Eu^{3+} emission is far less intense and the Tb/Eu emission ratio is larger for **r-LZF1$^{\mathbf{Tb|Cs124|Eu}}$** *vs* **r-LZF1$^{\mathbf{Eu|Cs124|Tb}}$** (Table 1). In agreement with our design, locating the Eu^{3+} at the N-terminus, closer to the antenna improves Eu^{3+} sensitization efficiency and corresponding emission intensity. When **r-LZF1$^{\mathbf{Eu|Cs124|Tb}}$** is titrated by Zn^{2+}, Tb^{3+} emission increases linearly with the amount of Zn^{2+} up to 1.0 eq. and plateaus above.

Zn^{2+}-binding causes an 11-fold increase of Tb^{3+} emission intensity, similar to the previously described intensiometric probe **LZF1**$^{Cs124|Tb}$ (13-fold increase).[30] Comparatively, the increase in Eu^{3+} emission intensity is less affected, *i.e.* only ca. 30 % increase, and the Eu^{3+} signal remains very weak in comparison to the one of Tb^{3+} (Figure 4B and Figure S9 of Supporting Information). Therefore, the evolution of Tb^{3+} and Eu^{3+} emissions upon Zn^{2+} addition differs markedly making **r-LZF1**$^{Eu|Cs124|Tb}$ a ratiometric probe. Nevertheless, Eu^{3+} emission is too weak and hardly detectable in comparison to Tb^{3+}, complicating practical use of this probe.

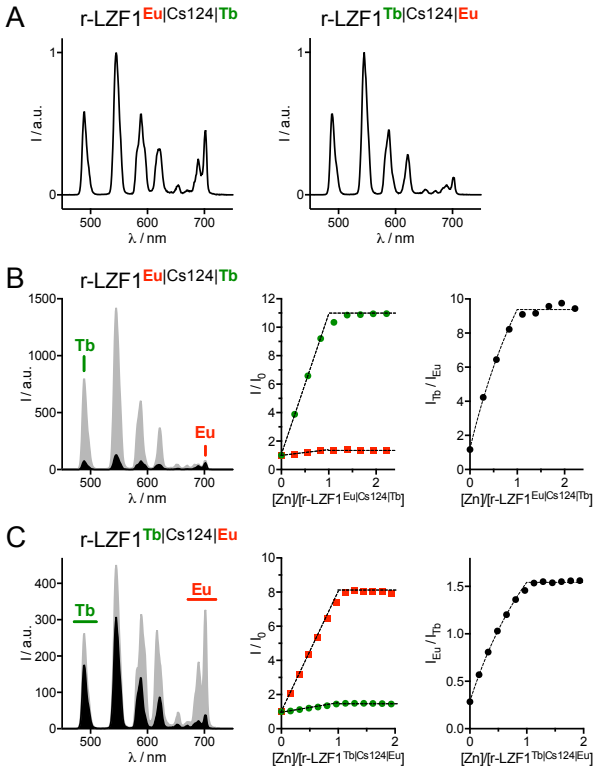

Figure 4: Time-gated luminescence spectroscopy (λ_{ex} = 330 nm, delay time = 100 µs, gate time = 2 ms) of visible-emitting ratiometric probes. (A) Normalized emission spectra of **r-LZF1**$^{Eu|Cs124|Tb}$ (*left*) and **r-LZF1**$^{Tb|Cs124|Eu}$ (*right*) in their Zn-free forms. (B) Emission spectra of **r-LZF1**$^{Eu|Cs124|Tb}$ in its Zn-free (black) and Zn-bound (grey) forms (*left*) and monitoring of Tb^{3+} (490 nm, green) and Eu^{3+} (702 nm, red) channels during a Zn^{2+} titration of **r-LZF1**$^{Eu|Cs124|Tb}$ (*middle*) and evolution of the emission ratio of the Tb^{3+} channel over the Eu^{3+} channel (*right*). (C) Emission spectra of **r-LZF1**$^{Tb|Cs124|Eu}$ in its Zn-free (black) and Zn-bound (grey) forms (*left*) and monitoring of integrated Tb^{3+} (470-510 nm, green) and Eu^{3+} (680-720 nm, red) channels during a Zn^{2+} titration of **r-LZF1**$^{Eu|Cs124|Tb}$ (*middle*) and evolution of the emission ratio of the Eu^{3+} channel over the Tb^{3+} channel (*right*). Solutions were prepared with 10 µM **r-LZF** probe in aerated HEPES buffer (10 mM, pH 7.5) containing TCEP (250 µM).

The overall behaviour of the other peptide **LZF1**$^{Tb|Cs124|Eu}$ is quite similar (Figure 4C and Figure S10 of Supporting Information) with a linear increase of both Tb^{3+} and Eu^{3+} emissions up to 1.0 eq. of Zn^{2+} but with an 8-fold increase of the Eu^{3+} emission and a much smaller (1.4-fold) increase of the Tb^{3+} signal providing a ratiometric response upon binding of one Zn^{2+} ion. However, compared to **r-LZF1**$^{Eu|Cs124|Tb}$, r-**LZF1**$^{Tb|Cs124|Eu}$ displays Tb^{3+} and Eu^{3+} emissions of comparable intensities allowing practical ratiometric detection of Zn^{2+} as confirmed by the evolution of the emission ratio of Eu^{3+} channel around 700 nm over Tb^{3+} channel around 490 nm (Figure 4C). For both peptides, Tb^{3+} and Eu^{3+} luminescence lifetimes for Zn-free probes were *ca.* 1.93 ±

0.03 ms and 0.65 ± 0.02 ms, respectively, and they remain unchanged for the Zn-bound peptide (Table 1 and Table S2 of Supporting Information). These luminescence lifetime values are typical of DOTA-monoamide Tb^{3+} and Eu^{3+} complexes in related mono-lanthanide peptide conjugates.[30,32,40] Complementary luminescence lifetimes measurements on **r-LZF1**$^{\mathbf{Tb|Cs124|Eu}}$ conducted in deuterated water shows that one water molecule is bound to Tb^{3+} or Eu^{3+} for both Zn-free and Zn-bound forms (Figure 17 of Supporting Information). Altogether, this result indicates that the ratiometric behaviour of **r-LZF1**$^{\mathbf{Eu|Cs124|Tb}}$ and **r-LZF1**$^{\mathbf{Tb|Cs124|Eu}}$ is caused only by the Zn^{2+}-induced peptide folding that shortens the distance between the antenna and the Ln^{3+} and that it is not due to a change in the Ln^{3+} hydration number or to a Tb^{3+}-to-Eu^{3+} energy transfer. Quantum yields of Ln^{3+} luminescence upon excitation of the Cs124 antenna (Table 1) are rather modest but similar to those of the related probe **LZF1**$^{\mathbf{Cs124|Tb}}$.[30] Finally, the dissociation constant (K_d) of the Zn·**r-LZF1**$^{\mathbf{Tb|Cs124|Eu}}$-complex was measured to be $10^{-9.2}$ by competitive Zn^{2+} titration using EGTA (ethylene glycol-bis(□-aminoethylether)-*N*,*N*,*N*',*N*'-tetraacetic acid) as a competitor (Figure S20 and Table S3 of Supporting Information). This value falls within the suitable range for detection of circulating Zn^{2+} in cells, where $[Zn^{2+}]$ lies between 10^{-11} and 10^{-8} M.[37,47] Hence, the design of **r-LZF1**$^{\mathbf{Tb|Cs124|Eu}}$ and its spectral behaviour in response to Zn^{2+} demonstrate that NCL gives access to hetero-bis-lanthanide peptide conjugates that can behave as ratiometric luminescent sensors. The comparison between **r-LZF1**$^{\mathbf{Eu|Cs124|Tb}}$ and **r-LZF1**$^{\mathbf{Tb|Cs124|Eu}}$ clearly indicates the importance of the location of each lanthanide relative to the antenna to adapt their emission range and to optimize the probe response.

Table 1: Summary of **r-LZF1**$^{\mathbf{Eu|Cs124|Tb}}$ and **r-LZF1**$^{\mathbf{Tb|Cs124|Eu}}$ probes characterizations: dissociation constants, terbium and europium luminescence enhancements, ratios of terbium over europium emission, quantum yields (Φ^{Ln}) and Ln^{3+} luminescence lifetimes.

	r-LZF1$^{\mathbf{Eu\|Cs124\|Tb}}$		**r-LZF1**$^{\mathbf{Tb\|Cs124\|Eu}}$	
log K_d	n.d.[a]		-9.2 ± 0.2	
I_{Zn}/I_0	Tb: 11	Eu: 1.3	Tb: 1.4	Eu: 8
Tb/Eu ratio[b]				
Zn-free	2.2		8.1	
Zn-bound	17.8		1.4	
Φ^{Ln} / %[c]				
Zn-free	0.13		0.24	
Zn-bound	1.6		0.60	
lifetimes / ms				
Zn-free	Tb: 1.96	Eu: 0.64	Tb: 1.93	Eu:0.66
Zn-bound	Tb: 1.92	Eu: 0.66	Tb: 1.91	Eu:0.67

[a] Not determined. [b] The Tb/Eu ratio was obtained by deconvolution of the emission spectra using spectra of related Tb- and Eu-DOTA-monoamide compounds, *i.e.* **LZF1**$^{\mathbf{Cs124|Tb}}$ and **LZF1**$^{\mathbf{Cs124|Eu}}$.[30] [c] λ_{ex} = 330 nm.

Toward NIR-emissive probes: screening of antennas for the sensitization of Nd^{3+} and Yb^{3+} luminescence

Besides the Tb^{3+}/Eu^{3+} pair, other pairs of lanthanides could be used to design ratiometric probes. Of special interest are NIR-emitting lanthanides, neodymium and ytterbium, which emit around 1000 nm (Figure 1). Therefore, our next challenge was the unprecedented design of a ratiometric probe based on these two lanthanides for ratiometric NIR detection. We have previously described that an amino-derivative of 7-nitro-2,1,3-benzoxadiazole (NBD) can sensitize Nd^{3+} luminescence and that **LZF1**$^{\mathbf{NBD|Nd}}$ featuring a Dap(NBD) amino acid and a DOTA-Nd^{3+} complex is a NIR-emitting intensiometric luminescent probe for the detection of Zn^{2+}.[30] Unfortunately, NBD is unable to sensitize Yb^{3+}. Therefore, we looked for antennas that could

sensitize both Nd^{3+} and Yb^{3+}. For this purpose, and to limit the synthetic effort, we decided to use once again NCL to perform this screening. We synthesized a series of N-terminal segments bearing a candidate antenna chromophore and two C-terminal segments bearing either a DOTA-Yb^{3+} or a DOTA-Nd^{3+} complex (Figure 5A). Note that C-terminal segment with both Dap or Lys anchorage for the DOTA chelator were used in this screening process, giving **LZF1** or **LZF3** probes, respectively. Indeed, we switched from Dap to Lys residue because the C-terminal segment with Lys anchorage was obtained in better yield. This structural variation has a minor impact on the probe properties as evidenced by comparison of **LZF3**$^{Cs124|Ln}$ probes (Ln = Tb or Eu) with the previously described **LZF1**$^{Cs124|Ln}$ probes[30] (Figure S18 and S19 of Supporting Information). For the implementation of this screening, we assessed the potential of five antennas for the sensitization of NIR-emitting Ln^{3+} through various chromophores absorbing in the UV or the visible ranges (Figure 5B): 4-(dimethylamino)-1,8-naphthalimide (4-DMN, λ_{max} = 447 nm), 1-amino-anthraquinone (AAQ, λ_{max} = 505 nm), 7-(diethylamino)-coumarin (DEAC, λ_{max} = 433 nm), a water-soluble derivative of 3,6-diphenyl-diketopyrrolopyrrole[48] (DPP, λ_{max} = 455 nm) and anthracene (Anthra, λ_{max} = 369 nm). The experimental procedures for the synthesis of the various **LZF1**$^{Antenna|Ln}$ or **LZF3**$^{Antenna|Ln}$ (Ln = Nd and Yb) peptides are described in the Supporting Information.

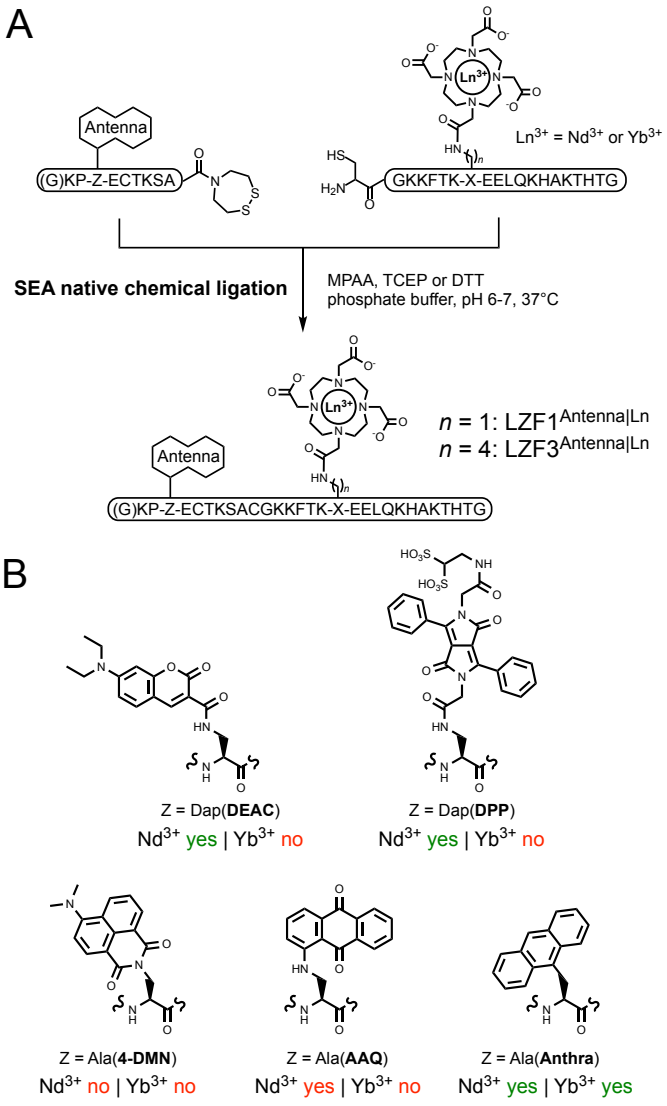

Figure 5: Screening of antennas for Nd^{3+} and Yb^{3+} sensitization by native chemical ligation. (A) Reaction scheme for the 2-segment peptide assembly by NCL. (B) Structures of antenna amino acids explored in this screening and summary of their ability to sensitize Nd^{3+} and Yb^{3+} luminescence.

Ln^{3+} complexes with a coordinated amido-derivative of anthraquinone have already been described to sensitize both Nd^{3+} and Yb^{3+} luminescence in deuterated water[49] and a remote 1,8-diamino-anthraquinone antenna has been shown to sensitize both lanthanides in methanol.[50] However, no sensitized NIR lanthanide luminescence could be detected for **LZF1$^{AAQ|Nd}$** or **LZF1$^{AAQ|Yb}$** with their amino-anthraquinone chromophore in buffered water (HEPES, pH 7.5). 4-Amino-1,8-naphthalimide has already been used by one of us as a sensitizing antenna for Nd^{3+} and Yb^{3+} in dendrimeric systems[51] but unfortunately, here again, neither Nd^{3+} nor Yb^{3+} luminescence could be observed for **LFZ3$^{4DMN|Ln}$** upon excitation of the chromophore. In contrast, **LZF1$^{DPP|Ln}$** (Figure S11 of Supporting Information) and **LFZ3$^{DEAC|Ln}$** (Figure S12 of Supporting Information) displayed sensitized Nd^{3+} emission but not the one arising from Yb^{3+}. Upon Zn^{2+} binding, the Nd^{3+} emission is increased *ca.* 3-fold for **LZF1$^{DPP|Nd}$** and 7-fold for **LFZ3$^{DEAC|Nd}$**, showing that these two peptides can operate as intensiometric probes for Zn^{2+} detection in the NIR. The fifth antenna to be assessed was anthracene, which has already been reported to successfully sensitize Nd^{3+}, Yb^{3+} and Er^{3+} NIR luminescence in dichloromethane solution or in the solid state.[52,53] Indeed, with **LZF3$^{Anthra|Nd}$** and **LZF3$^{Anthra|Yb}$**, anthracene was able to sensitize both lanthanides upon excitation in the 330-400 nm spectral range and both peptides show a weak lanthanide luminescence increase upon zinc binding, *i.e.* 1.3 and 1.5-fold for Nd^{3+} and Yb^{3+}, respectively (Figure 6 and Figure S13 and S14 of Supporting Information). The quantum yields of Ln^{3+} luminescence upon antenna (DPP, DEAC or Anthra) excitation (Table S1 of Supporting Information) are in the same order of magnitude as the one of the previously described **LZF1$^{NBD|Nd}$** probe, *i.e.* 10^{-4} – 6×10^{-3} %. From this screening study, it appears that anthracene is a suitable antenna for both Nd^{3+} and Yb^{3+} in our peptide-based system. Thus, it appeared to be a promising candidate for the design of a dual-wavelength NIR-emitting ratiometric probes. Therefore, the hetero-bis-lanthanide peptides **r-LZF3$^{Yb|Anthra|Nd}$** and **r-LZF3$^{Nd|Anthra|Yb}$** (Figure 2B) were assembled by NCL of a N-terminal segment bearing a DOTA-Ln^{3+} complex and the anthracene antenna and a C-terminal segment bearing the second DOTA-Ln^{3+} complex, as described in Figure 3.

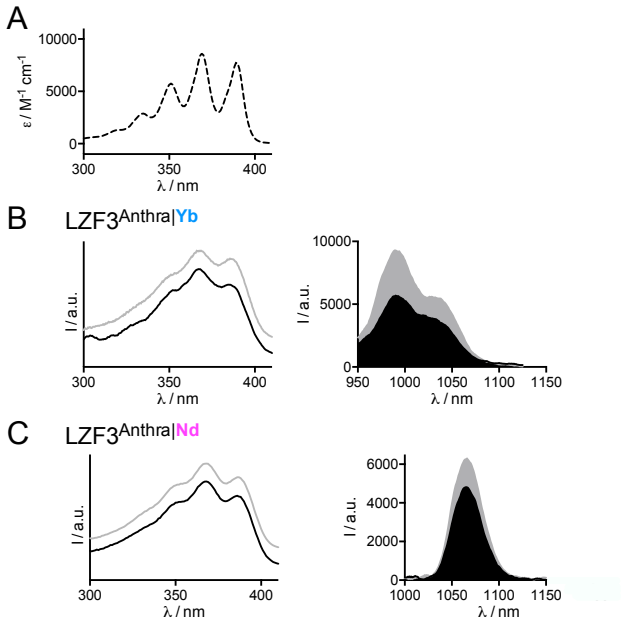

Figure 6: (A) Absorption spectrum of the anthracene antenna. (B,C) Excitation (λ_{em} = 990 nm for Yb^{3+} and 1060 nm for Nd^{3+}) and emission (λ_{ex} = 370 nm) spectra of (B) **LZF3$^{Athra|Yb}$** and (C) **LZF3$^{Athra|Nd}$** in their Zn-free (black) and Zn-bound (grey) forms. Solutions were prepared with 50 µM probe in degassed HEPES buffer (10 mM, pH 7.5).

Characterization of ratiometric probes emitting in the NIR

The luminescence properties of **r-LZF3**$^{\mathbf{Nd|Anthra|Yb}}$ and **r-LZF3**$^{\mathbf{Yb|Anthra|Nd}}$ were investigated in degassed HEPES buffer at pH 7.5. Upon excitation of the anthracene chromophore at 370 nm, both **r-LZF3**$^{\mathbf{Nd|Anthra|Yb}}$ and **r-LZF3**$^{\mathbf{Yb|Anthra|Nd}}$ display the characteristic emission signals of Yb^{3+} and Nd^{3+} (Figure 7) with similar intensities (see Nd/Yb ratio in Table 2). Addition of Zn^{2+} up to 1.0 eq. leads to an overall emission increase (Figure 7 and Figure S15 and S16 of Supporting Information). In the case of **r-LZF3**$^{\mathbf{Nd|Anthra|Yb}}$, emission of both Yb^{3+} and Nd^{3+} increase in a similar extent, *i.e.* 1.8 and 1.5-fold for Yb^{3+} and Nd^{3+}, respectively, making ratiometric detection difficult (Figure 7A). Conversely, the other peptide, **r-LZF3**$^{\mathbf{Yb|Anthra|Nd}}$, displays an increase of the Nd^{3+} emission only, while the one of Yb^{3+} remains constant, making the ratiometric detection obvious as seen in Figure 7B. The quantum yields of Ln^{3+} emission of these two ratiometric probes (Table 2) are comparable to those of **LZF3**$^{\mathbf{Antra|Nd}}$ and **LZF3**$^{\mathbf{Antra|Yb}}$ (Table S1 of Supporting Information). The dissociation constant (K_d) of the Zn·**r-LZF3**$^{\mathbf{Yb|Anthra|Nd}}$ complex was determined to be $10^{-10.8}$ by competitive Zn^{2+} titration using EGTA (Figure S20 of Supporting Information), in line with the lower K_d for probes containing a Lys(DOTA-Ln) residue with respect to Dap(DOTA-Ln), as observed for **LZF1**$^{\mathbf{Cs124|Ln}}$ *vs* **LZF3**$^{\mathbf{Cs124|Ln}}$ probes (Figure S20 and Table S3 of Supporting Information). To the best of our knowledge, **r-LZF3**$^{\mathbf{Yb|Anthra|Nd}}$ constitute the first proof-of-principle responsive and lanthanide-based ratiometric probe with dual-wavelength emission in the NIR.

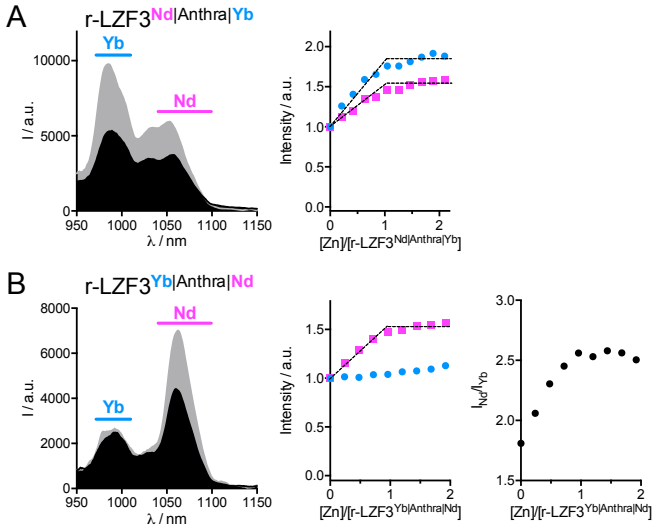

Figure 7: Luminescence spectroscopy (λ_{ex} = 370 nm) of NIR-emitting ratiometric probes. (A) Emission spectra of **r-LZF3**$^{\mathbf{Nd|Athra|Yb}}$ in its Zn-free (black) and Zn-bound (grey) forms (*left*) and monitoring of Yb^{3+} (970-1010 nm, blue) and Nd^{3+} (1040-1100 nm, pink) channels during a Zn^{2+} titration of **r-LZF3**$^{\mathbf{Nd|Anhra|Yb}}$ (*right*). (B) Emission spectra of **r-LZF3**$^{\mathbf{Yb|Anthra|Nd}}$ in its Zn-free (black) and Zn-bound (grey) forms (*left*) and monitoring of integrated Yb^{3+} (970-1010 nm, blue) and Nd^{3+} (1040-1100 nm, pink) channels during a Zn^{2+} titration of **r-LZF3**$^{\mathbf{Yb|Anhtra|Nd}}$ (*middle*) and evolution of the emission ratio of the Nd^{3+} channel over the Yb^{3+} channel. Solutions were prepared with 25 µM probe in degassed HEPES buffer (10 mM, pH 7.5).

Table 2: Summary of **r-LZF3**$^{\mathbf{Nd|Anthra|Yb}}$ and **r-LZF3**$^{\mathbf{Yb|Anthra|Nd}}$ probes characterizations: dissociation constant, ytterbium and neodymium luminescence enhancement, ratio of neodymium over ytterbium emission in the spectra.

	r-LZF3$^{\mathbf{Nd|Anthra|Yb}}$		**r-LZF1**$^{\mathbf{Yb|Anthra|Nd}}$	
log K_d	n.d.[a]		-10.8 ± 0.2	
I_{Zn}/I_0	Yb: 1.8	Nd: 1.5	Yb: 1.0	Nd: 1.5
Nd/Yb ratio[b]				
Zn-free	0.44		1.6	
Zn-bound	0.33		2.6	
Φ^{Ln} / %[c]				
Zn-free	4.4×10^{-3}		3.9×10^{-3}	
Zn-bound	6.6×10^{-3}		4.7×10^{-3}	

[a] Not determined. [b] The Nd/Yb ratio was obtained by deconvolution of the emission spectra using spectra of the related Yb- and Nd-DOTA-monoamide compounds **LZF3**$^{\mathbf{Anthra|Yb}}$ and **LZF3**$^{\mathbf{Anthra|Nd}}$. [c] λ_{ex} = 370 nm.

Conclusions

In summary, we have demonstrated that hetero-bis-lanthanide peptide conjugates site-specifically labeled with two distinct Ln^{3+} within the same molecule framework can be easily prepared by native chemical ligation of two peptide segments, each bearing a distinct kinetically and thermodynamically-stable DOTA-Ln^{3+} complex. As a proof-of-concept of this strategy, we have created several zinc-responsive probes with dual-wavelength ratiometric emission in the visible or in the NIR. Among them, **r-LZF1**$^{\mathbf{Tb|Cs124|Eu}}$ and **r-LZF3**$^{\mathbf{Yb|Anthra|Nd}}$ display ratiometric detection properties in response to the presence of Zn^{2+} with visible (480-710 nm) and NIR (950-1150 nm) emission signals, respectively. These two probes clearly demonstrate that NCL is an attractive and efficient approach to properly design ratiometric luminescent lanthanide-based probes.

Acknowledgment

Authors acknowledge the Agence Nationale de la Recherche (ANR-12-BS07-0012 and ANR-13-BSV5-009), La Ligue Contre le Cancer, Le Cancéropôle Grand Ouest, La Region Centre and the Labex ARCANE and CBH-EUR-GS (ANR-17-EURE-0003) for financial support. S.P. acknowledges support from the Institut National de la Santé et de la Recherche Médicale (INSERM). A.R. thank the French "Investissements d'Avenir" program, project ISITE-BFC (contract ANR-15-IDEX-0003), for its financial support for research in the field of DPP-based fluorophores for biosensing/bioimaging.

References

[1] E. Haustein, P. Schwille, *HFSP J.* **2007**, *1*, 169, DOI: 10.2976/1.2778852.
[2] H. Kobayashi, M. Ogawa, R. Alford, P. L. Choyke, Y. Urano, *Chem. Rev.* **2010**, *110*, 2620, DOI: 10.1021/cr900263j.
[3] T. Nagaya, Y. A. Nakamura, P. L. Choyke, H. Kobayashi, *Front. Oncol.* **2017**, *7*, 314, DOI: 10.3389/fonc.2017.00314.
[4] C. H. F. Wenk, F. Ponce, S. Guillermet, C. Tenaud, D. Boturyn, P. Dumy, D. Watrelot-Virieux, C. Carozzo, V. Josserand, J.-L. Coll, *Cancer Lett.* **2013**, *334*, 188, DOI: 10.1016/j.canlet.2012.10.041.
[5] T. Ueno, T. Nagano, *Nat. Methods* **2011**, *8*, 642, DOI: 10.1038/nmeth.1663.

[6] J. Zhou, H. Ma, *Chem. Sci.* **2016**, *7*, 6309, DOI: 10.1039/C6SC02500E.
[7] H. Zhu, J. Fan, J. Du, X. Peng, *Acc. Chem. Res.* **2016**, *49*, 2115, DOI: 10.1021/acs.accounts.6b00292.
[8] A. Kaur, J. L. Kolanowski, E. J. New, *Angew. Chem., Int. Ed.* **2016**, *55*, 1602, DOI: 10.1002/anie.201506353.
[9] D. Andina, J.-C. Leroux, P. Luciani, *Chem.-Eur. J.* **2017**, *23*, 13549, DOI: 10.1002/chem.201702458.
[10] J. Zhang, X. Chai, X.-P. He, H.-J. Kim, J. Yoon, H. Tian, *Chem. Soc. Rev.* **2019**, *48*, 683, DOI: 10.1039/C7CS00907K.
[11] O. Tagit, N. Hildebrandt, *ACS Sens.* **2017**, *2*, 31, DOI: 10.1021/acssensors.6b00625.
[12] M. H. Lee, J. S. Kim, J. L. Sessler, *Chem. Soc. Rev.* **2015**, *44*, 4185, DOI: 10.1039/C4CS00280F.
[13] C. P. Montgomery, B. S. Murray, E. J. New, R. Pal, D. Parker, *Accounts Chem. Res.* **2009**, *42*, 925, DOI: 10.1021/ar800174z.
[14] M. C. Heffern, L. M. Matosziuk, T. J. Meade, *Chem. Rev.* **2014**, *114*, 4496, DOI: 10.1021/cr400477t.
[15] M. Sy, A. Nonat, N. Hildebrandt, L. J. Charbonnière, *Chem. Commun.* **2016**, *52*, 5080, DOI: 10.1039/C6CC00922K.
[16] J.-C. G. Bünzli, *J. Lumin.* **2016**, *170*, 866, DOI: 10.1016/j.jlumin.2015.07.033.
[17] K. Y. Zhang, Q. Yu, H. Wei, S. Liu, Q. Zhao, W. Huang, *Chem. Rev.* **2018**, *118*, 1770, DOI: 10.1021/acs.chemrev.7b00425.
[18] J.-C. G. Bünzli, S. V. Eliseeva, in 'Lanthanide Luminescence', Eds. P. Hänninen, H. Härmä, Springer Berlin Heidelberg, **2011**, pp. 1.
[19] Y. Bretonniere, M. J. Cann, D. Parker, R. Slater, *Org. Biomol. Chem.* **2004**, *2*, 1624, DOI: 10.1039/B400734B.
[20] R. Pal, D. Parker, *Chem. Commun.* **2007**, 474, DOI: 10.1039/b616665b.
[21] D. G. Smith, B. K. McMahon, R. Pal, D. Parker, *Chem. Commun.* **2012**, *48*, 8520, DOI: 10.1039/c2cc34267g.
[22] L. B. Jennings, S. Shuvaev, M. A. Fox, R. Pal, D. Parker, *Dalton Trans.* **2018**, *47*, 16145, DOI: 10.1039/C8DT03823F.
[23] S. J. Butler, *Chem. Commun.* **2015**, *51*, 10879, DOI: 10.1039/C5CC03428K.
[24] E. A. Weitz, J. Y. Chang, A. H. Rosenfield, E. A. Morrow, V. C. Pierre, *Chem. Sci.* **2013**, *4*, 4052, DOI: 10.1039/C3SC51583D.
[25] M. S. Tremblay, M. Halim, D. Sames, *J. Am. Chem. Soc.* **2007**, *129*, 7570, DOI: 10.1021/ja070867y.
[26] G.-L. Law, R. Pal, L. O. Palsson, D. Parker, K.-L. Wong, *Chem. Commun.* **2009**, 7321, DOI: 10.1039/b920222f.
[27] D. G. Smith, R. Pal, D. Parker, *Chem.-Eur. J.* **2012**, *18*, 11604, DOI: 10.1002/chem.201201738.
[28] C. Song, Z. Ye, G. Wang, J. Yuan, Y. Guan, *Chem.-Eur. J.* **2010**, *16*, 6464, DOI: 10.1002/chem.201000528.
[29] Z. Dai, L. Tian, B. Song, Z. Ye, X. Liu, J. Yuan, *Anal. Chem.* **2014**, *86*, 11883, DOI: 10.1021/ac503611f.
[30] M. Isaac, L. Raibaut, C. Cepeda, A. Roux, D. Boturyn, S. V. Eliseeva, S. Petoud, O. Sénèque, *Chem.-Eur. J.* **2017**, *23*, 10992, DOI: 10.1002/chem.201703089.
[31] M. S. Tremblay, D. Sames, *Chem. Commun.* **2006**, 4116, DOI: 10.1039/b607949k.
[32] T. J. Sørensen, A. M. Kenwright, S. Faulkner, *Chem. Sci.* **2015**, *6*, 2054, DOI: 10.1039/C4SC03827D.
[33] P. E. Dawson, T. W. Muir, I. Clarklewis, S. B. H. Kent, *Science* **1994**, *266*, 776, DOI: 10.1126/science.7973629.
[34] V. Agouridas, O. El Mahdi, V. Diemer, M. Cargoët, J.-C. M. Monbaliu, O. Melnyk, *Chem. Rev.* **2019**, *119*, 7328, DOI: 10.1021/acs.chemrev.8b00712.
[35] W. Maret, *Met. Ions Life Sci.* **2013**, *12*, 479, DOI: 10.1007/978-94-007-5561-1_14.
[36] K. P. Carter, A. M. Young, A. E. Palmer, *Chem. Rev.* **2014**, *114*, 4564, DOI: 10.1021/cr400546e.
[37] A. M. Hessels, M. Merkx, *Metallomics* **2015**, *7*, 258, DOI: 10.1039/C4MT00179F.
[38] Y. Chen, Y. Bai, Z. Han, W. He, Z. Guo, *Chem. Soc. Rev.* **2015**, *44*, 4517, DOI: 10.1039/C5CS00005J.
[39] S.-H. Park, N. Kwon, J.-H. Lee, J. Yoon, I. Shin, *Chem. Soc. Rev.* **2020**, *49*, 143, DOI: 10.1039/C9CS00243J.
[40] M. Isaac, A. Pallier, F. Szeremeta, P.-A. Bayle, L. Barantin, C. S. Bonnet, O. Sénèque, *Chem. Commun.* **2018**, *54*, 7350, DOI: 10.1039/C8CC04366C.
[41] M. Isaac, S. A. Denisov, A. Roux, D. Imbert, G. Jonusauskas, N. D. McClenaghan, O. Sénèque, *Angew. Chem., Int. Ed.* **2015**, *54*, 11453, DOI: 10.1002/anie.201505733.
[42] A. Roux, M. Isaac, V. Chabert, S. A. Denisov, N. D. McClenaghan, O. Sénèque, *Org. Biomol. Chem.* **2018**, *16*, 5626, DOI: 10.1039/C8OB01044G.
[43] L. Raibaut, W. Vasseur, G. D. Shimberg, C. Saint-Pierre, J.-L. Ravanat, S. L. J. Michel, O. Sénèque,

Chem. Sci. **2017**, *8*, 1658, DOI: 10.1039/C6SC04086A.
[44] M. Li, P. R. Selvin, *J. Am. Chem. Soc.* **1995**, *117*, 8132, DOI: 10.1021/ja00136a010.
[45] G. S. Beligere, P. E. Dawson, *Peptide Sci.* **1999**, *51*, 363.
[46] S. Futaki, K. Tatsuto, Y. Shiraishi, Y. Sugiura, *Peptide Sci.* **2004**, *76*, 98, DOI: 10.1002/bip.10562.
[47] W. Maret, *Metallomics* **2015**, *7*, 202, DOI: 10.1039/C4MT00230J.
[48] E. Heyer, P. Lory, J. Leprince, M. Moreau, A. Romieu, M. Guardigli, A. Roda, R. Ziessel, *Angew. Chem., Int. Ed.* **2015**, *54*, 2995, DOI: 10.1002/anie.201411274.
[49] J. E. Jones, S. J. A. Pope, *Dalton Trans.* **2009**, 8421, DOI: 10.1039/b913902h.
[50] O. J. Stacey, B. D. Ward, A. J. Amoroso, S. J. A. Pope, *Dalton Trans.* **2016**, *45*, 6674, DOI: 10.1039/C5DT04351D.
[51] A. Foucault-Collet, Ph.D. Thesis Université d'Orléans, Orléans, **2013**.
[52] T. Lazarides, M. A. H. Alamiry, H. Adams, S. J. A. Pope, S. Faulkner, J. A. Weinstein, M. D. Ward, *Dalton Trans.* **2007**, 1484, DOI: 10.1039/b700714k.
[53] B. Casanovas, S. Speed, O. Maury, M. S. E. Fallah, M. Font-Bardía, R. Vicente, *Eur. J. Inorg. Chem.* **2018**, *2018*, 3859, DOI: 10.1002/ejic.201800624.

Using Native Chemical Ligation for Site-specific Synthesis of Hetero-bis-lanthanide Peptide Conjugates: Application to Ratiometric Visible or Near-infrared Detection of Zn^{2+}

Céline Cepeda,[ab] Laurent Raibaut,[a] Guillaume Fremy,[ab] Svetlana V. Eliseeva,[c] Anthony Romieu,[d] Jacques Pécaut,[e] Didier Boturyn,[b] Stéphane Petoud,*[c] and Olivier Sénèque*[a]

[a] Univ. Grenoble Alpes, CNRS, CEA, IRIG, LCBM (UMR 5249), F-38000 Grenoble, France.

[b] Univ. Grenoble Alpes, CNRS, DCM (UMR 5250) F-38000 Grenoble, France.

[c] Centre de Biophysique Moléculaire, UPR CNRS 4301, Université d'Orléans, rue Charles Sadron, F-45071 Orléans, France.

[d] ICMUB, UMR 6302, CNRS, Univ. Bourgogne Franche-Comté, 9 Avenue Alain Savary, 21000 Dijon, France.

[e] Univ. Grenoble Alpes, CEA, CNRS, IRIG, SyMMES, F-38000 Grenoble, France.

Email: *olivier.seneque@cea.fr* and *stephane.petoud@inserm.fr*

Supporting Information

Content

Abbreviations

AAQ: 1-aminoanthraquinone; AcOH: acetic acid; AcOEt: ethyl acetate; Alloc: allyloxycarbonyl; Boc: *tert*-butyloxycarbonyl; Cs124: carbostyril 124; Dap: diaminopropionic acid; DCM: dicholoromethane; DEAC: 7-dimethylamino-coumarin-3-carboxy; diamide: *N*,*N*,*N*′,*N*′-tetramethylazodicarboxamide; DIEA: *N*,*N*-diisopropyl-ethylamine; DOTA: 1,4,7,10-tetraazacyclododecane-1,4,7,10-tetraacetic acid; DMF: *N*,*N*-dimethylformamide; 4-DMN: *N*,*N'*-dimethyl-1,8-naphthalimido; DMSO: dimethylsulfoxide; DTT: dithiothreitol; EDTA, ethylenediamine-tetraacetic acid; EGTA: ethylene glycol-*bis*(2-aminoethylether)-*N*,*N*,*N*′,*N*′-tetraacetic acid; ESI: electrospray ionization; Et_2O: diethylether; Fmoc: 9-fluorenyl-methoxycarbonyl; ; Fmoc-OSu: Fmoc *N*-hydroxysuccinimide ester; HATU: *N*-[(dimethylamino)-*1H*-1,2,3-triazolo[4,5-b]-pyridin-1-ylmethylene]-*N*-methylmethanaminium hexafluoro-phosphate N-oxide; HEDTA: *N*-hydroxyethyl-ethylenediamine-triacetic acid; HPLC: high performance liquid chromatography; LRMS: low resolution mass spectrometry; MeCN: acetonitrile; MPAA: 4-mercaptophenylacetic acid; NH_4OAc: ammonium acetate; $Pd(PPh_3)_4$: *tetrakis*(triphenylphosphine)palladium(0); PyBOP: (benzotriazol-1-yloxy)tripyrrolidinophosphonium-hexafluoro-phosphate; SEA: *bis*(2-sulfanyl-ethyl)amino; SEA-PS: (*bis*(2-sulfanyl-ethyl)-amino)-2-chlorotrityl-polystyrene; TCEP: *tris*(2-carboxyethyl)phosphine; TFA: trifluoroacetic acid; TIS: triisopropylsilane; *t*Bu: *tert*-butyl; Trt: trityl; UV-Vis: ultraviolet-visible.

Materials and methods

Reagents and solvents: N-α-Fmoc-protected amino acids for peptide synthesis, PyBOP and HATU coupling reagents were obtained from Novabiochem or Iris Biotech. Fmoc-L-Glu(Cs124)-OH and Fmoc-L-Ala(4-DMN)-OH and disulfonated 3,6-diphenyl-DPP dye (abbreviated as DPP-OH in this article) were synthetized according to literature procedures.[1–3] Fmoc-3-(9-anthryl)-L-Ala-OH was purchased from Santa Cruz Biotechnology. SEA-PS and NovaPEG Rink Amide resin were purchased from X'prochem and Novabiochem, respectively. DOTA-*tris*(*t*Bu)ester was purchased from CheMatech. Other reagents for peptide synthesis, solvents, buffers and metal salts were purchased from Sigma-Aldrich. All buffer or metal solutions for spectroscopic measurements were prepared with ultrapure water produced by a Millipore Milli-Q® purification system (purified to 18.2 MΩ.cm). The concentration of the Zn^{2+} solution was determined by colorimetric EDTA titrations.[4] Buffer solutions were treated with Chelex 100 resin (Bio-Rad) to remove trace metal ions.

Characterization and purification: Analytical HPLC separations were performed on an Agilent Infinity 1260 system using Merck Chromolith RP-18e (100 mm × 4.6 mm) columns at a flow rate of 2 mL/min. Preparative HPLC separations were performed on a VWR LaPrepΣ system using Waters XBridge Peptide BEH130 C18 (5 µm, 150 mm × 19 mm) or Waters XBridge Peptide BEH130 C18 (5 µm, 150 mm × 10 mm) columns at flow rates of 14 or 6 mL/min, respectively. Mobile phase consisted in a gradient of solvent A (0.1% TFA in H_2O) and B (0.1% TFA in MeCN/H_2O 9:1). For analytical separations, Method A consisted in 5% B during 1 min followed by a 5 to 50 % B linear gradient in 14 min at 2 mL/min and Method B consisted in 5% B during 1 min followed by a 5 to 100 % B gradient in 14 min at 2 mL/min. Eluate was monitored by electronic absorption at 214, 280 and 331 nm. ESI-MS analyses were performed on a Thermo LXQ spectrometer. UV-Vis absorption spectra were recorded on a Perkin-Elmer Lambda 35 spectrophotometer equipped with a thermo-regulated cell holder.

Amino acid synthesis

***N*-α-Boc-3-(1-anthraquinone-amino)-L-Ala-OH:** To a solution of Boc-Dap-OH (500 mg, 2.45 mmol) and DIEA (1.9 mL, 11 mmol) in H_2O/DMF 1:1 (36 mL) was added 1-chloroanthraquinone (297 mg, 1.2 mmol) and $CuSO_4$ (586 mg, 3.7 mmol). The reaction mixture was stirred for 24 h on reflux. The solvents were removed under reduced pressure and the oily residue was dissolved in DCM, washed twice with 0.01 M aq. HCl, then twice with 1 mM aq. NaOH. DCM was added to the basic aqueous phases and 0.1 M aq. HCl was added to adjust the pH of the aqueous layer to 3. The organic layer was separated, dried over anhydrous Na_2SO_4 and evaporated under reduced pressure to give the desired product as a red solid (27 mg, 0.07 mmol, 5.6 %). ^{1}H NMR (200 MHz, 298 K, $CDCl_3$): δ = 9.89 (s, 1H), 8.14 (m, 2H), 7.66 (t, 2H), 7.56-7.44 (m, 2H), 7.16 (d, *J* = 7.5 Hz, 1H), 5.60 (d, *J* = 7.6 Hz, 1H), 4.66 (m, 1H), 3.83 (br, 2H), 1.45 (s, 9H) ppm; HPLC (anal.): t_R = 9.8 min (method B); LRMS (ESI+): monoisotopic *m/z* = 411.0 (+) / calculated monoisotopic *m/z* = 411.16 $[M+H]^+$ for M = $C_{22}H_{22}N_2O_6$.

***N*-α-Fmoc-3-(1-anthraquinone-amino)-L-Ala-OH:** Boc-3-(1-anthraquinone-amino)-L-Ala-OH (58 mg, 140 µmol) was dissolved in DCM/TFA 1:1 (10 mL) and stirred at room temperature for 2 h. The solvents were removed under reduced pressure. The residue was triturated in Et_2O and the supernatant was removed (three times). The solid was dried under vacuum. It was then dissolved in H_2O (3 mL) with K_2CO_3 (29 mg, 275 µmol). Then a solution of Fmoc-OSu (70 mg, 185 µmol) in 1,4-dioxane (6 mL) was added. After 30 minutes on stirring, H_2O (25 mL) was added and the aqueous solution was washed twice with Et_2O (150 mL). The aqueous layer was acidified to pH 3 with 2 M aq. HCl and extracted with AcOEt. The organic layer was dried over anhydrous Na_2SO_4 and evaporated under reduced pressure. The residue was sequentially triturated in toluene, Et_2O and acetone to give the desired *N*-Fmoc amino acid as a red solid (78 mg, 146 µmol, 78 %). ^{1}H NMR (400 MHz, 298 K, acetone-d_6): δ = 10.01 (br t, 1H), 8.17 (m, 2H), 7.86-7.74 (m, 4H), 7.73-7.61 (m, 3H), 7.55 (d, *J* = 6.9 Hz, 1H), 7.46-731 (m, 3H), 7.26 (t, *J* = 6.9 Hz, 2H), 7.10 (d, *J* = 7.0 Hz, 1H), 4.67 (m, 1H), 4.45-4.17 (m, 3H), 4.05 (m, 1H), 3.87 (m, 1H) ppm; ^{13}C NMR (100 MHz, 298 K, acetone-d_6): δ = 185.6, 183.8, 172.0, 157.2, 157.1, 152.4, 145.1, 145.0, 142.1, 136.4, 135.7, 135.6, 134.1, 133.8, 128.5, 127.9, 127.5, 127.2, 126.2, 126.1, 120.7, 118.9, 116.5, 114.3, 67.5, 54.4, 48.0, 44.5 ppm; HPLC (anal.): t_R = 10.4 min (method B); LRMS (ESI–): monoisotopic *m/z* = 531.1 (–) / calculated monoisotopic *m/z* = 531.16 $[M–H]^–$ for M = $C_{32}H_{24}N_2O_6$.

Peptide sequences

1a^{Cs124}:[5] Ac-Gly-Lys-Pro-Glu(Cs124)-Glu-Cys(S*t*Bu)-Thr-Lys-Ser-Ala-SEA^{off}
1a^{DEAC}: Ac-Lys-Pro-Dap(DEAC)-Glu-Cys(S*t*Bu)-Thr-Lys-Ser-Ala-SEA^{off}
1a^{DPP}: Ac-Lys-Pro-Dap(DPP)-Glu-Cys(S*t*Bu)-Thr-Lys-Ser-Ala-SEA^{off}
1a^{DMN}: Ac-Lys-Pro-Ala(4-DMN)-Glu-Cys(S*t*Bu)-Thr-Lys-Ser-Ala-SEA^{off}
1a^{AAQ}: Ac-Lys-Pro-Ala(AAQ)-Glu-Cys(S*t*Bu)-Thr-Lys-Ser-Ala-SEA^{off}
1a^{Anthra}: Ac-Gly-Lys-Pro-Ala(9-anthryl)-Glu-Cys(S*t*Bu)-Thr-Lys-Ser-Ala-SEA^{off}
1b^{Cs124}: DOTA-Gly-Lys-Pro-Glu(Cs124)-Glu-Cys(S*t*Bu)-Thr-Lys-Ser-Ala-SEA^{off}
1b$^{Tb|Cs124}$: DOTA[Tb]-Gly-Lys-Pro-Glu(Cs124)-Glu-Cys(S*t*Bu)-Thr-Lys-Ser-Ala-SEA^{off}
1b$^{Eu|Cs124}$: DOTA[Eu]-Gly-Lys-Pro-Glu(Cs124)-Glu-Cys(S*t*Bu)-Thr-Lys-Ser-Ala-SEA^{off}
1b^{Anthra}: DOTA-Gly-Lys-Pro-Ala(9-anthryl)-Glu-Cys(S*t*Bu)-Thr-Lys-Ser-Ala-SEA^{off}
1b$^{Nd|Anthra}$: DOTA[Nd]-Gly-Lys-Pro-Ala(9-anthryl)-Glu-Cys(S*t*Bu)-Thr-Lys-Ser-Ala-SEA^{off}
1b$^{Yb|Anthra}$: DOTA[Yb]-Gly-Lys-Pro-Ala(9-anthryl)-Glu-Cys(S*t*Bu)-Thr-Lys-Ser-Ala-SEA^{off}

2a:[5] Cys-Gly-Lys-Lys-Phe-Thr-Lys-Dap(DOTA)-Glu-Glu-Leu-Gln-Lys-His-Ala-Lys-Thr-His-Thr-Gly-NH_2
2a^{Tb}:[5] Cys-Gly-Lys-Lys-Phe-Thr-Lys-Dap(DOTA[Tb])-Glu-Glu-Leu-Gln-Lys-His-Ala-Lys-Thr-His-Thr-Gly-NH_2
2a^{Eu}:[5] Cys-Gly-Lys-Lys-Phe-Thr-Lys-Dap(DOTA[Eu])-Glu-Glu-Leu-Gln-Lys-His-Ala-Lys-Thr-His-Thr-Gly-NH_2
2aNd:[5] Cys-Gly-Lys-Lys-Phe-Thr-Lys-Dap(DOTA[Nd])-Glu-Glu-Leu-Gln-Lys-His-Ala-Lys-Thr-His-Thr-Gly-NH_2
2a^{Yb}: Cys-Gly-Lys-Lys-Phe-Thr-Lys-Dap(DOTA[Yb])-Glu-Glu-Leu-Gln-Lys-His-Ala-Lys-Thr-His-Thr-Gly-NH_2
2b: Cys-Gly-Lys-Lys-Phe-Thr-Lys-Lys(DOTA)-Glu-Glu-Leu-Gln-Lys-His-Ala-Lys-Thr-His-Thr-Gly-NH_2
2b^{Tb}: Cys-Gly-Lys-Lys-Phe-Thr-Lys-Lys(DOTA[Tb])-Glu-Glu-Leu-Gln-Lys-His-Ala-Lys-Thr-His-Thr-Gly-NH_2
2b^{Eu}: Cys-Gly-Lys-Lys-Phe-Thr-Lys-Lys(DOTA[Eu])-Glu-Glu-Leu-Gln-Lys-His-Ala-Lys-Thr-His-Thr-Gly-NH_2
2bNd: Cys-Gly-Lys-Lys-Phe-Thr-Lys-Lys(DOTA[Nd])-Glu-Glu-Leu-Gln-Lys-His-Ala-Lys-Thr-His-Thr-Gly-NH_2
2b^{Yb}: Cys-Gly-Lys-Lys-Phe-Thr-Lys-Lys(DOTA[Yb])-Glu-Glu-Leu-Gln-Lys-His-Ala-Lys-Thr-His-Thr-Gly-NH_2

LZF3$^{Cs124|Tb}$: Ac-Gly-Lys-Pro-Glu(Cs124)-Glu-Cys-Thr-Lys-Ser-Ala-Cys-Gly-Lys-Lys-Phe-Thr-Lys-Lys(DOTA[Tb])-Glu-Glu-Leu-Gln-Lys-His-Ala-Lys-Thr-His-Thr-Gly-NH_2
LZF3$^{Cs124|Eu}$: Ac-Gly-Lys-Pro-Glu(Cs124)-Glu-Cys-Thr-Lys-Ser-Ala-Cys-Gly-Lys-Lys-Phe-Thr-Lys-Lys(DOTA[Eu])-Glu-Glu-Leu-Gln-Lys-His-Ala-Lys-Thr-His-Thr-Gly-NH_2
LZF1$^{AAQ|Nd}$: Ac-Lys-Pro-Ala(AAQ)-Glu-Cys-Thr-Lys-Ser-Ala-Cys-Gly-Lys-Lys-Phe-Thr-Lys-Dap(DOTA[Nd])-Glu-Glu-Leu-Gln-Lys-His-Ala-Lys-Thr-His-Thr-Gly-NH_2
LZF1$^{AAQ|Yb}$: Ac-Lys-Pro-Ala(AAQ)-Glu-Cys-Thr-Lys-Ser-Ala-Cys-Gly-Lys-Lys-Phe-Thr-Lys-Dap(DOTA[Yb])-Glu-Glu-Leu-Gln-Lys-His-Ala-Lys-Thr-His-Thr-Gly-NH_2
LZF1$^{DPP|Nd}$: Ac-Lys-Pro-Dap(DPP)-Glu-Cys-Thr-Lys-Ser-Ala-Cys-Gly-Lys-Lys-Phe-Thr-Lys-Dap(DOTA[Nd])-Glu-Glu-Leu-Gln-Lys-His-Ala-Lys-Thr-His-Thr-Gly-NH_2
LZF1$^{DPP|Yb}$: Ac-Lys-Pro-Dap(DPP)-Glu-Cys-Thr-Lys-Ser-Ala-Cys-Gly-Lys-Lys-Phe-Thr-Lys-Dap(DOTA[Yb])-Glu-Glu-Leu-Gln-Lys-His-Ala-Lys-Thr-His-Thr-Gly-NH_2

LZF3$^{DEAC|Nd}$: Ac-Lys-Pro-Dap(DEAC)-Glu-Cys-Thr-Lys-Ser-Ala-Cys-Gly-Lys-Lys-Phe-Thr-Lys-Lys(DOTA[Nd])-Glu-Glu-Leu-Gln-Lys-His-Ala-Lys-Thr-His-Thr-Gly-NH_2
LZF3$^{DEAC|Yb}$: Ac-Lys-Pro-Dap(DEAC)-Glu-Cys-Thr-Lys-Ser-Ala-Cys-Gly-Lys-Lys-Phe-Thr-Lys-Lys(DOTA[Yb])-Glu-Glu-Leu-Gln-Lys-His-Ala-Lys-Thr-His-Thr-Gly-NH_2
LZF3$^{DMN|Nd}$: Ac-Lys-Pro-Ala(4-DMN)-Glu-Cys-Thr-Lys-Ser-Ala-Cys-Gly-Lys-Lys-Phe-Thr-Lys-Lys(DOTA[Nd])-Glu-Glu-Leu-Gln-Lys-His-Ala-Lys-Thr-His-Thr-Gly-NH_2
LZF3$^{DMN|Yb}$: Ac-Lys-Pro-Ala(4-DMN)-Glu-Cys-Thr-Lys-Ser-Ala-Cys-Gly-Lys-Lys-Phe-Thr-Lys-Lys(DOTA[Yb])-Glu-Glu-Leu-Gln-Lys-His-Ala-Lys-Thr-His-Thr-Gly-NH_2

LZF3$^{Anthra|Nd}$: Ac-Gly-Lys-Pro-Ala(9-anthryl)-Glu-Cys-Thr-Lys-Ser-Ala-Cys-Gly-Lys-Lys-Phe-Thr-Lys-Lys(DOTA[Nd])-Glu-Glu-Leu-Gln-Lys-His-Ala-Lys-Thr-His-Thr-Gly-NH_2
LZF3$^{Anthra|Yb}$: Ac-Gly-Lys-Pro-Ala(9-anthryl)-Glu-Cys-Thr-Lys-Ser-Ala-Cys-Gly-Lys-Lys-Phe-Thr-Lys-Lys(DOTA[Yb])-Glu-Glu-Leu-Gln-Lys-His-Ala-Lys-Thr-His-Thr-Gly-NH_2

r-LZF1$^{Eu|Cs124|Tb}$: DOTA[Eu]-Gly-Lys-Pro-Glu(Cs124)-Glu-Cys-Thr-Lys-Ser-Ala-Cys-Gly-Lys-Lys-Phe-Thr-Lys-Dap(DOTA[Tb])-Glu-Glu-Leu-Gln-Lys-His-Ala-Lys-Thr-His-Thr-Gly-NH_2
r-LZF1$^{Tb|Cs124|Eu}$: DOTA[Tb]-Gly-Lys-Pro-Glu(Cs124)-Glu-Cys-Thr-Lys-Ser-Ala-Cys-Gly-Lys-Lys-Phe-Thr-Lys-Dap(DOTA[Eu])-Glu-Glu-Leu-Gln-Lys-His-Ala-Lys-Thr-His-Thr-Gly-NH_2

r-LZF3$^{Yb|Anthra|Nd}$: DOTA[Yb]-Gly-Lys-Pro-Ala(9-anthryl)-Glu-Cys-Thr-Lys-Ser-Ala-Cys-Gly-Lys-Lys-Phe-Thr-Lys-Lys(DOTA[Nd])-Glu-Glu-Leu-Gln-Lys-His-Ala-Lys-Thr-His-Thr-Gly-NH_2
r-LZF3$^{Nd|Anthra|Yb}$: DOTA[Nd]-Gly-Lys-Pro-Ala(9-anthryl)-Glu-Cys-Thr-Lys-Ser-Ala-Cys-Gly-Lys-Lys-Phe-Thr-Lys-Lys(DOTA[Yb])-Glu-Glu-Leu-Gln-Lys-His-Ala-Lys-Thr-His-Thr-Gly-NH_2

Peptide synthesis

Peptide elongation: Peptide elongation was performed using standard SPPS procedure using Fmoc/*t*Bu chemistry either manually or on an automated peptide synthesizer (CEM Liberty1 Microwave Peptide Synthesizer). Double couplings (30 min) were performed using 4-fold molar excess of Fmoc-L-amino acid, 4-fold molar excess of PyBOP and 8-fold molar excess of DIEA at room temperature. A capping step was performed after each coupling with Ac_2O/DIEA in DMF (5 min). Fmoc removal was performed using 20% piperidine in DMF (2×10 min).

SEA^{off} N-terminal segments 1:

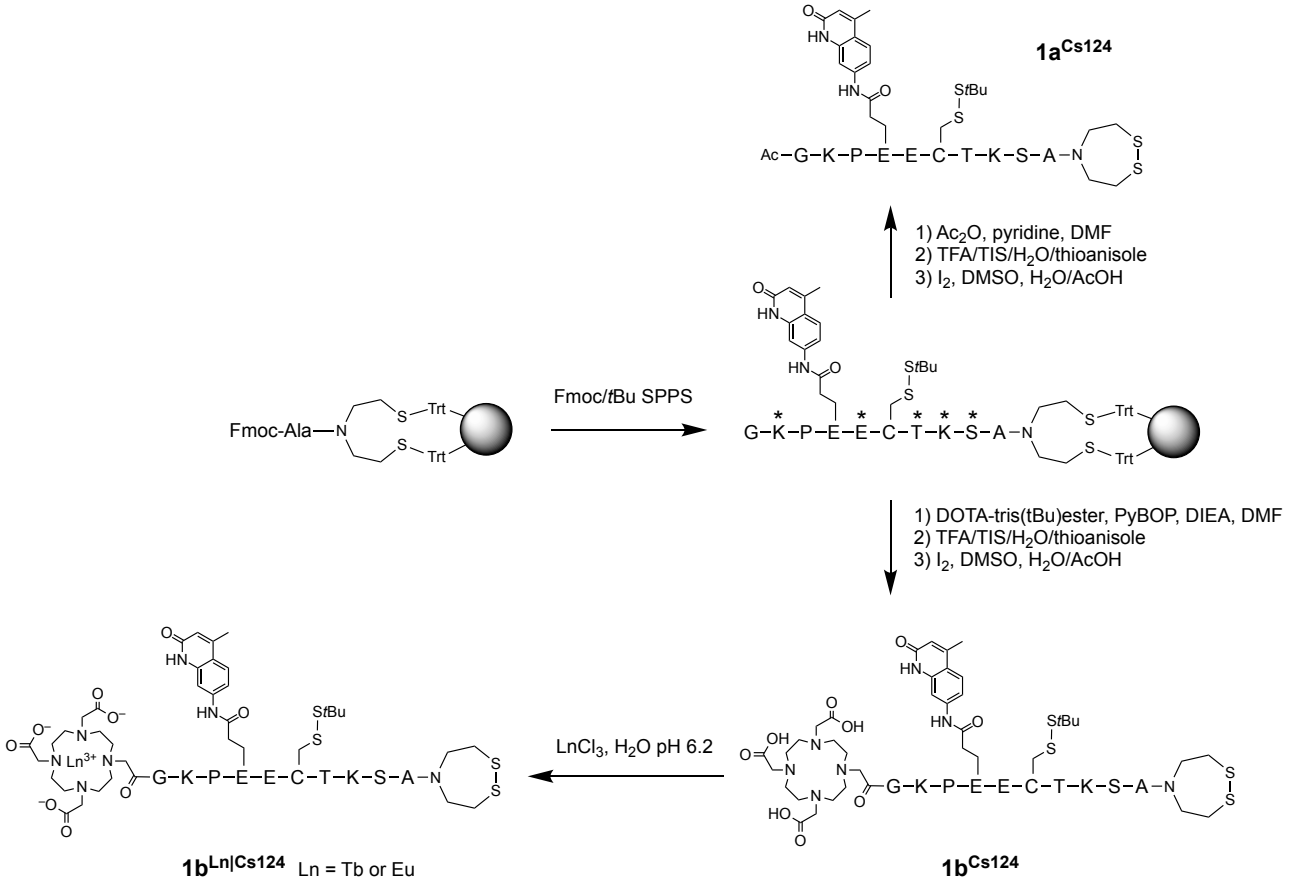

Figure S1. Synthetic pathway for the preparation of **1a^{Cs124}** and **1b$^{Ln|Cs124}$** (Ln = Tb or Eu). * denotes standard side chain protecting group (Boc for Lys; *t*Bu for Glu, Thr and Ser).

1a^{Cs124}: The synthesis was performed as described previously.[5]

1b^{Cs124}: Peptide elongation was performed as described above on SEA-PS resin (0.025 mmol, 0.16 mmol/g) after attachment of the first amino acid by double manual coupling (30 min) using 10-fold excess of Fmoc-Ala-OH, 9.5-fold excess of HATU and 10-fold excess of DIEA in DMF with pre-activation (5 min) followed by acetylation using Ac_2O/DIEA/DCM (2:1:17 v/v/v, 10 mL, 2×5 min).[6] Non-standard Fmoc-L-Cys(S*t*Bu)-OH amino acid was used to introduce the cysteine residue. Fmoc-L-Glu(Cs124)-OH[1] was used to introduce the antenna. DOTA-*tris*(*t*Bu)ester (3 eq.) was coupled overnight to the N-terminus using PyBOP (3 eq.) activation with DIEA (6 eq.) in DMF (5 mL). Removal of acid-labile side chain protecting groups and cleavage of the peptidyl resin was performed with TFA/H_2O/TIS/thioanisole (92.5:2.5:2.5:2.5 v/v/v/v, 10 mL) during 2 h. The peptide was then precipitated in ice-cold Et_2O/heptane (1:1 v/v, 100 mL), dissolved in H_2O, and lyophilized. The peptide was dissolved in H_2O/AcOH and treated with a solution of I_2 (200 mM in DMSO) to oxidize the C-terminal SEA^{on} group into SEA^{off} group.[6,7] After 30 s, DTT (65 mM in H_2O, 500 µL) was added to quench the excess of iodine. The oxidized peptide was immediately purified by HPLC to give fragment **1b**

as a powder (10 mg, 21 % yield for the **1b^{Cs124}**·(TFA)$_2$ salt). HPLC (anal.): t_R = 10.3 min (method A); LRMS (ESI+): monoisotopic *m/z* = 1797.7 (+), 898.9 (2+), 599.8 (3+) / calculated monoisotopic *m/z* = 1796.78 $[M+H]^+$, 898.90 $[M+2H]^{2+}$, 599.60 $[M+3H]^{3+}$ for M = $C_{76}H_{121}N_{19}O_{23}S_4$.

Formation of Ln^{3+} complexes 1b$^{Ln|Cs124}$ (Ln = Tb, Eu): Compound **1b^{Cs124}** (2.5 µmol, 5 mg) was dissolved in H_2O and the pH was adjusted to 6.2 using NaOH. Then, the lanthanide salt $LnCl_3$ (10 µmol) was added. The solution was stirred overnight under argon (after 1h, the pH was controlled and adjusted to 6.2 if needed). TCEP (35 µmol, 10 mg) was added prior to removal of excess Ln^{3+} by HPLC purification. The Ln-loaded peptide was obtained as a white powder after freeze-drying (85-90% yield).

1b$^{Tb|Cs124}$: HPLC (anal.): t_R = 9.8 min (method A); LRMS (ESI+): average *m/z* = 1953.5 (+), 977.3 (2+), 651.9 (3+) / calculated av. *m/z* = 1954.06 $[M+H]^+$, 977.54 $[M+2H]^{2+}$, 652.03 $[M+3H]^{3+}$ for M = $C_{76}H_{118}N_{19}O_{23}S_4Tb$).

1b$^{Eu|Cs124}$: HPLC (anal.): t_R = 9.8 min (method A); LRMS (ESI+): average *m/z* = 1946.5 (+), 974.1 (2+), 649.8 (3+) / calculated av. *m/z* = 1947.10 $[M+H]^+$, 974.06 $[M+2H]^{2+}$, 649.71 $[M+3H]^{3+}$ for M = $C_{76}H_{118}N_{19}O_{23}S_4Eu$).

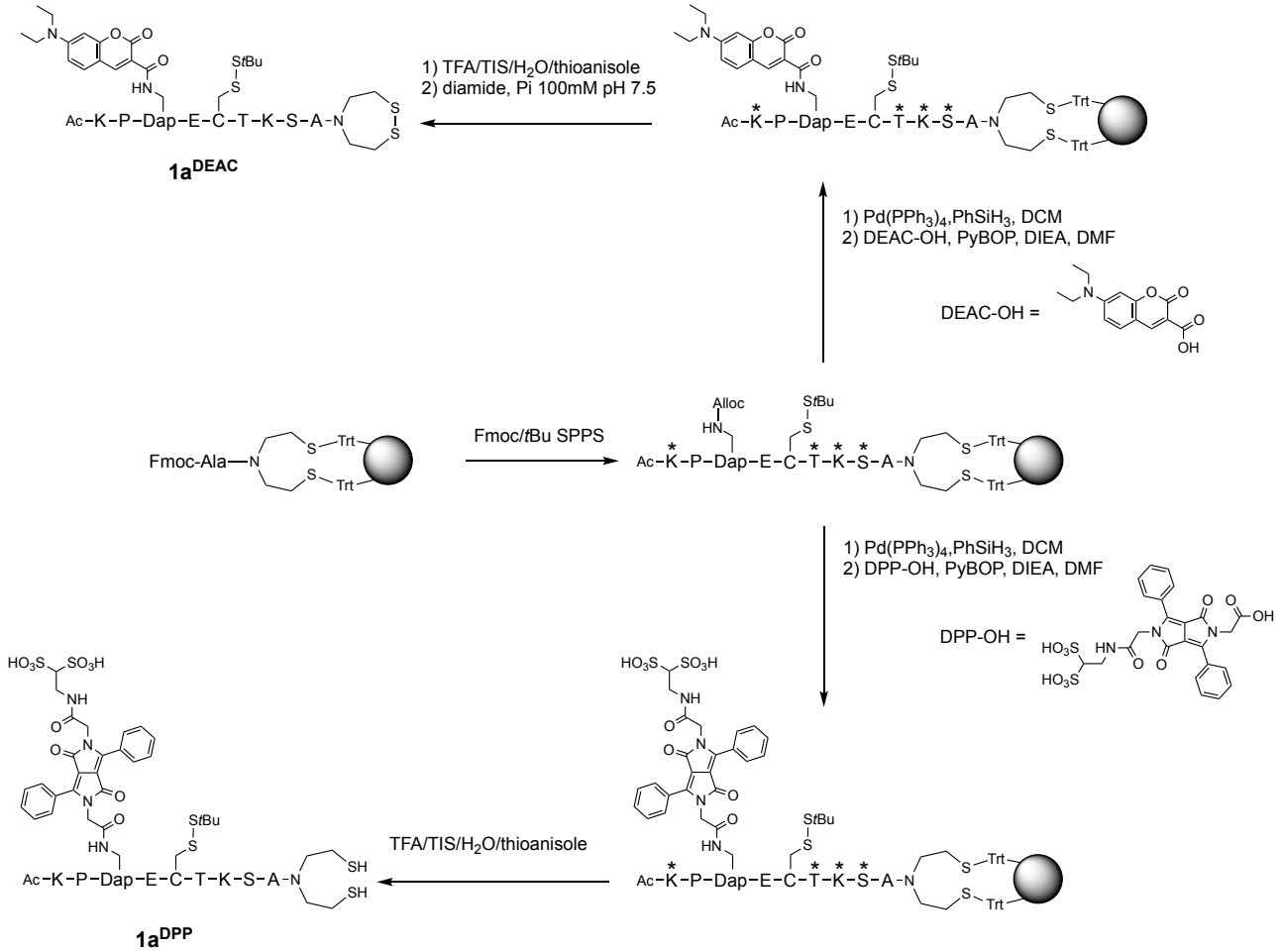

Figure S2. Synthetic pathway for the preparation of **1a^{DEAC}** and **1a^{DPP}**. * denotes standard side chain protecting group (Boc for Lys; *t*Bu for Glu, Thr and Ser).

1a^{DEAC}: Peptide elongation was performed as described above on SEA-PS resin (0.1 mmol, 0.16 mmol/g) after attachment of the first amino acid by double manual coupling (30 min) using 10-fold excess of Fmoc-L-Ala-OH, 9.5-fold excess of HATU and 10-fold excess of DIEA in DMF with pre-activation (5 min) followed by acetylation using Ac_2O/DIEA/DCM (2:1:17 v/v/v, 10 mL, 2×5 min).[6] Fmoc-L-Dap(Alloc)-OH and Fmoc-L-Cys(S*t*Bu)-OH amino acids were used to introduce the diaminopropionic acid and cysteine residues, respectively. After acetylation of the N-terminus, removal of

the N-Alloc protecting group of the Dap(Alloc) residue was performed by adding a solution of $Pd(PPh_3)_4$ (0.05 mmol, 0.5 eq., 58 mg) and phenylsilane (2.5 mmol, 25 eq., 0.3 mL) in degassed anhydrous DCM (15 mL) for 1 h in the dark (twice).[8] The resin was then washed successively with DCM (2×2 min), DMF (2×2 min), 1% H_2O in DMF (2×2 min), DMF (2×2 min), 1% DIEA in DMF (2×2 min), DMF (2×2 min), sodium diethyldithiocarbamate in DMF (0.12 M, 2×5 min) and DMF (2×2 min). The rest of the synthesis was performed on three tenth of the resin (0.03 mmol scale). A solution of 7-(dimethylamino)-coumarin-3-carboxylic acid (0.09 mmol, 23.5 mg, 3 eq.), PyBOP (0.09 mmol, 46.8 mg, 3 eq.) and DIEA (0.18 mmol, 32 µL, 6 eq.) in DMF (8 mL) was prepared and added to the resin. The resin was agitated 2 h at room temperature. The resin was washed with DMF (2×2 min), DCM (2×2 min) and Et_2O (2×2 min) and dried. Removal of acid-labile side chain protecting groups and cleavage of the peptidyl resin was performed with TFA/H_2O/TIS/thioanisole (92.5:2.5:2.5:2.5 v/v/v, 10 mL) during 2 h. The peptide was then precipitated in ice-cold Et_2O/heptane (1:1 by vol., 100 mL), dissolved in H_2O, and lyophilized. The crude peptide was dissolved in phosphate buffer 0.1 M pH 7.5 (1 mg/mL) and treated with diamide to oxidize the C-terminal SEA^{on} group into SEA^{off} group.[6,7] After 1 h on stirring, the oxidized peptide was purified by HPLC to give fragment $\mathbf{1a^{DEAC}}$ as a powder (15.5 mg, 31 % yield for the $\mathbf{1a^{DEAC}}$·$(TFA)_2$ salt). HPLC (anal.): t_R = 12.6 min (method A); LRMS (ESI+): monoisotopic *m/z* = 1439.4 (+), 720.4 (2+) / calculated monoisotopic *m/z* = 1439.62 $[M+H]^+$, 720.31 $[M+2H]^{2+}$ for M = $C_{62}H_{98}N_{14}O_{17}S_4$.

$\mathbf{1a^{DPP}}$ (SEA^{on} form): Peptide elongation on SEA-PS resin (0.1 mmol, 0.16 mmol/g) and Alloc removal were performed as described above for $1a^{DEAC}$. The rest of the synthesis was performed on one tenth of the resin (0.01 mmol scale). A solution of DPP-OH[3] (0.02 mmol, 11.8 mg, 2 eq.), PyBOP (0.03 mmol, 15.6 mg, 3 eq.) and DIEA (0.08 mmol, 14 µL, 8 eq.) in DMF (8 mL) was prepared and added to the resin (0.01 mmol scale). The resin was agitated overnight at room temperature and the coupling step was repeated once for 4 h. The resin was washed with DMF (2×2 min), DCM (2×2 min) and Et_2O (2×2 min) and dried. Removal of acid-labile side chain protecting groups and cleavage of the peptidyl resin was performed with TFA/H_2O/TIS/thioanisole (92.5:2.5:2.5:2.5 v/v/v/v, 10 mL) during 2 h. The peptide was then precipitated in ice-cold Et_2O/heptane (1:1 v/v, 100 mL), dissolved in H_2O, and lyophilized (8 mg). Due to its instability to I_2 or diamide treatment, this compound was not converted into the SEA^{off} form and it was used without further purification. HPLC (anal.): t_R = 11.1 min (method A); LRMS (ESI+): average *m/z* = 1774 (+), 887 (2+) / calculated average *m/z* = 1773.11 $[M+H]^+$, 887.06 $[M+2H]^{2+}$ for M = $C_{72}H_{106}N_{16}O_{24}S_6$.

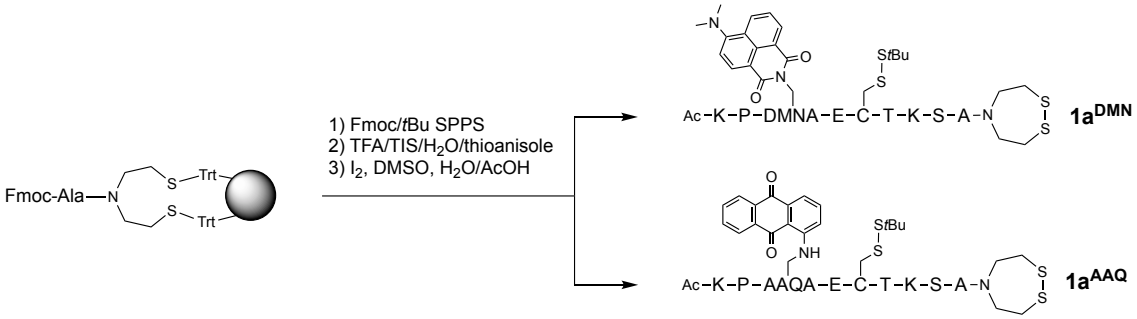

Figure S3. Synthetic pathway for the preparation of $\mathbf{1a^{DMN}}$ and $\mathbf{1a^{AAQ}}$. DMNA denotes 3-(4-*N*,*N*-dimethylamino-1,8-naphthalimido)-L-alanine and AAQA denotes 3-(1-anthraquinone-amino)-L-alanine. * denotes standard side chain protecting group (Boc for Lys; *t*Bu for Glu, Thr and Ser).

$\mathbf{1a^{DMN}}$: Peptide elongation was performed as described above on SEA-PS resin (0.03 mmol, 0.16 mmol/g) after attachment of the first amino acid by double manual coupling (30 min) using 10-fold excess of Fmoc-L-Ala-OH, 9.5-fold excess of HATU and 10-fold excess of DIEA in DMF with pre-activation (5 min) followed by acetylation using Ac_2O/DIEA/DCM (2:1:17 v/v/v, 10 mL, 2×5 min).[6] Non-standard Fmoc-L-Cys(S*t*Bu)-OH amino acid was used to introduce the cysteine residue and Fmoc-3-(4-*N*,*N*-dimethylamino-1,8-naphthalimido)-L-Ala-OH[2] was used to introduce the antenna. After acetylation of the N-terminus, removal of acid-labile side chain protecting groups and cleavage of the

peptidyl resin was performed with TFA/H_2O/TIS/thioanisole (92.5:2.5:2.5:2.5 v/v/v/v, 10 mL) during 2 h. The peptide was then precipitated in ice-cold Et_2O/heptane (1:1 v/v, 100 mL), dissolved in H_2O, and lyophilized. The peptide was dissolved in H_2O/AcOH and treated with a solution of I_2 (200 mM in DMSO) to oxidize the C-terminal SEA^{on} group into SEA^{off} group.[6,7] After 30 s, DTT (65 mM in H_2O, 500 µL) was added to quench the excess of iodine. The oxidized peptide was immediately purified by HPLC to give fragment **1a^{DMN}** as a powder (13.8 mg, 28 % yield for the **1a^{DMN}**·$(TFA)_2$ salt). HPLC (anal.): t_R = 7.4 min (method B); LRMS (ESI+): monoisotopic *m/z* = 1419.4 (+), 710.3 (2+) / calculated monoisotopic *m/z* = 1419.59 $[M+H]^+$, 710.30 $[M+2H]^{2+}$ for M = $C_{62}H_{94}N_{14}O_{16}S_4$.

1a^{AAQ}: Peptide elongation was performed as described above on SEA-PS resin (0.03 mmol, 0.16 mmol/g) after attachment of the first amino acid by double manual coupling (30 min) using 10-fold excess of Fmoc-L-Ala-OH, 9.5-fold excess of HATU and 10-fold excess of DIEA in DMF with pre-activation (5 min) followed by acetylation using Ac_2O/DIEA/DCM (2:1:17 v/v/v, 10 mL, 2×5 min).[6] Non-standard Fmoc-L-Cys(S*t*Bu)-OH amino acid was used to introduce the cysteine residue and Fmoc-3-(1-anthraquinone-amino)-L-Ala-OH was used to introduce the antenna. After acetylation of the N-terminus, removal of acid-labile side chain protecting groups and cleavage of the peptidyl resin was performed with TFA/H_2O/TIS/thioanisole (92.5:2.5:2.5:2.5 v/v/v/v, 10 mL) during 2 h. The peptide was then precipitated in ice-cold Et_2O/heptane (1:1 by vol., 100 mL), dissolved in H_2O, and lyophilized. The crude peptide was dissolved in phosphate buffer 0.1 M pH 7.5 (1 mg/mL) and treated with diamide to oxidize the C-terminal SEA^{on} group into SEA^{off} group.[6,7] After 10 min on stirring, the oxidized peptide was purified by HPLC to give fragment **1a^{AAQ}** as a powder (11 mg, 22 % yield for the **1a^{AAQ}**·$(TFA)_2$ salt). HPLC (anal.): t_R = 12.7 min (method A); LRMS (ESI+): monoisotopic *m/z* = 1402.3 (+), 701.7 (2+) / calculated monoisotopic *m/z* = 1402.57 $[M+H]^+$, 701.79 $[M+2H]^{2+}$ for M = $C_{62}H_{91}N_{13}O_{16}S_4$.

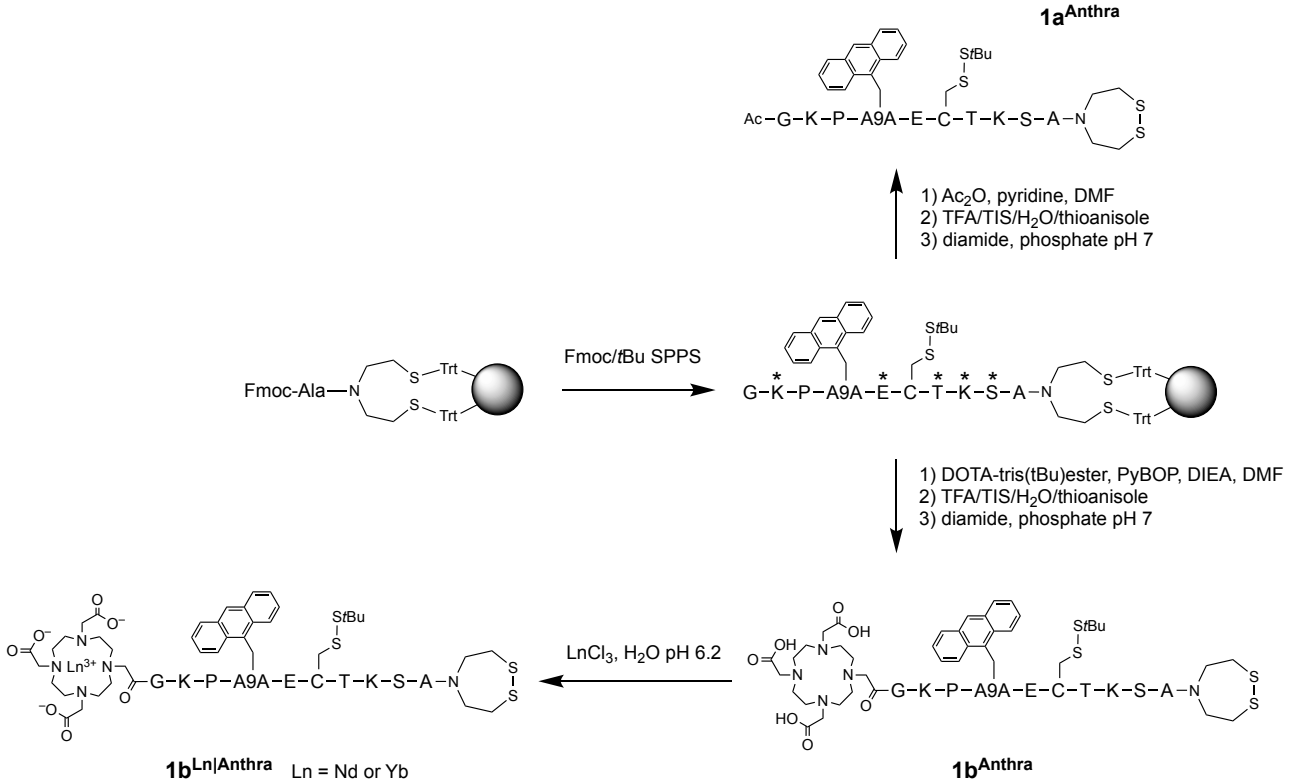

Figure S4. Synthetic pathway for the preparation of **1a^{Anthra}** and **1b$^{Ln|Anthra}$** (Ln = Nd or Yb). A9A denotes 3-(9-anthryl)-L-alanine. * denotes standard side chain protecting group (Boc for Lys; *t*Bu for Glu, Thr and Ser).

1a/b^{Anthra}: Peptide elongation was performed as described above on SEA-PS resin (0.06 mmol, 0.16 mmol/g) after attachment of the first amino acid by double manual coupling (30 min) using 10-fold excess of Fmoc-L-Ala-OH, 9.5-fold excess of HATU and 10-fold excess of DIEA in DMF with pre-activation (5 min) followed by acetylation using Ac_2O/DIEA/DCM (2:1:17 v/v/v, 10 mL, 2×5 min).[6] Non-standard Fmoc-L-Cys(S*t*Bu)-OH amino acid was used to introduce the cysteine residue. Fmoc-3-(9-anthryl)-L-Ala-OH was used to introduce the antenna. The resin was split into two equal parts. For 1a^{Anthra}, the N-terminus was acetylated. For 1b^{Anthra}, DOTA-*tris*(*t*Bu)ester (2 eq.) was coupled overnight to the N-terminus using PyBOP (2 eq.) activation with DIEA (6 eq.) in DMF (5 mL). Removal of acid-labile side chain protecting groups and cleavage of the peptidyl resin was performed with TFA/H_2O/TIS/thioanisole (92.5:2.5:2.5:2.5 v/v/v/v, 10 mL) during 4 h. The peptide was then precipitated in ice-cold Et_2O/heptane (1:1 v/v, 100 mL), dissolved in H_2O, and lyophilized. The peptide was dissolved in phosphate buffer (1 mg/mL) and treated with diamide (5 eq.) was added to oxidize the C-terminal SEA^{on} group into SEA^{off} group.[6,7] The oxidized peptide was immediately purified by HPLC to give fragment **1a/b** as a powder.

1a^{Anthra}: 17 mg (0.03 mmol scale), 35 % yield for the 1a^{Anthra}·$(TFA)_2$ salt. HPLC (anal.): t_R = 12.2 min (method A); LRMS (ESI+): monoisotopic *m/z* = 1415.5 (+), 707.9 (2+) / calculated monoisotopic *m/z* = 1414.60 $[M+H]^+$, 707.80 $[M+2H]^{2+}$ for M = $C_{64}H_{95}N_{13}O_{15}S_4$.

1b^{Anthra}: 17 mg (0.03 mmol scale), 29% yield for the 1b^{Anthra}·$(TFA)_2$ salt. HPLC (anal.): t_R = 12.3 min (method A); LRMS (ESI+): monoisotopic *m/z* = 1758.8 (+), 879.9 (2+), 586.9 (3+) / calculated monoisotopic *m/z* = 1758.77 $[M+H]^+$, 879.89 $[M+2H]^{2+}$, 586.93 $[M+3H]^{3+}$ for M = $C_{78}H_{119}N_{17}O_{21}S_4$.

Formation of Ln^{3+} complexes 1b$^{Ln|Anthra}$ (Ln = Nd or Yb): Metalation of **1b^{Anthra}** with Ln^{3+} was performed as described above for **1b$^{Ln|Cs124}$**.

1b$^{Nd|Anthra}$: HPLC (anal.): t_R = 9.8 min (method A); LRMS (ESI+): average *m/z* = 1900.5 (+), 950.6 (2+), 634.1 (3+) / calculated av. *m/z* = 1901.37 $[M+H]^+$, 951.19 $[M+2H]^{2+}$, 634.46 $[M+3H]^{3+}$ for M = $C_{78}H_{116}N_{17}O_{21}S_4Nd$).

1b$^{Yb|Anthra}$: HPLC (anal.): t_R = 9.8 min (method A); LRMS (ESI+): average *m/z* = 1929.7 (+), 965.6 (2+) / calculated av. *m/z* = 1930.17 $[M+H]^+$, 965.59 $[M+2H]^{2+}$ for M = $C_{78}H_{116}N_{17}O_{21}S_4Yb$).

C-terminal segments 2:

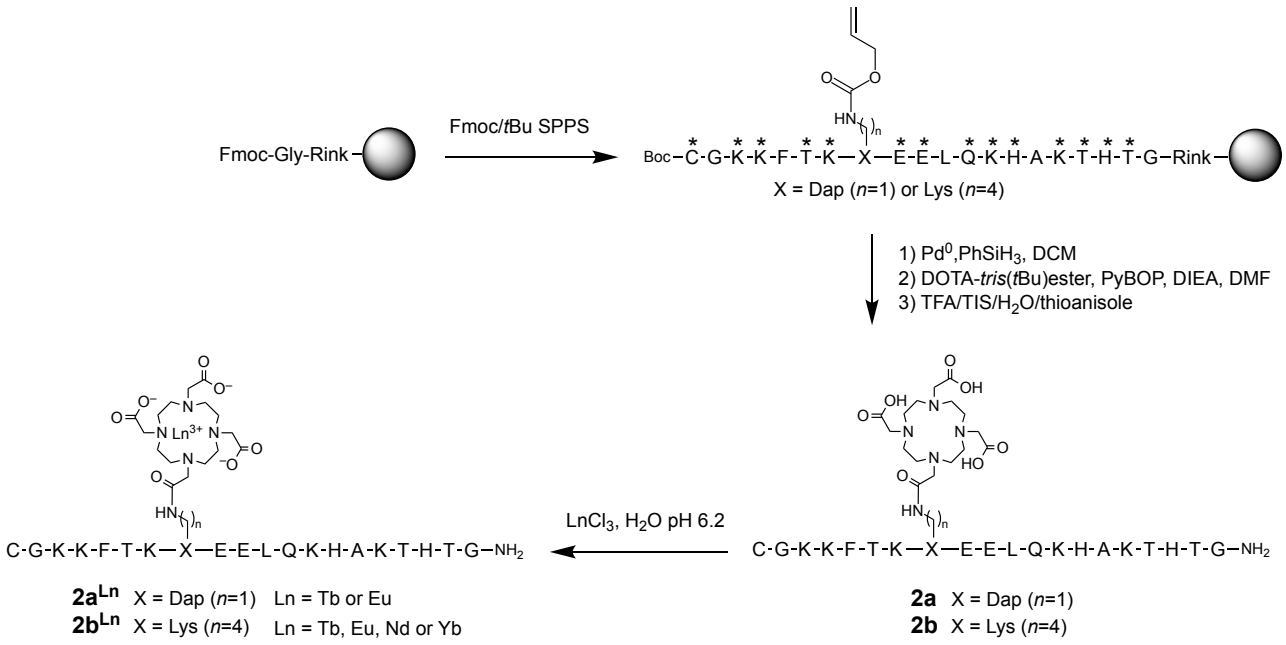

Figure S5. Synthetic pathway for the preparation of **2a^{Ln}** (Ln = Tb or Eu) and **2b^{Ln}** (Ln = Tb, Eu, Nd or Yb). * denotes standard side chain protecting group (Boc for Lys; *t*Bu for Glu, Thr and Ser; Trt for Cys, Gln and His).

$2a^{Ln}$ (Ln = Tb, Eu, Nd, Yb): The synthesis was performed as described previously.[5]

2b: Peptide elongation was performed as described above using a peptide synthesizer on Rink-PEG-PS resin (Nova PEG Rink Amide, 0.1 mmol, 0.45 mmol/g) after attachment of the first amino acid by single manual coupling (30 min) using 2-fold excess of Fmoc-Gly-OH, 2-fold excess of PyBOP and 6-fold excess of DIEA in DMF followed by acetylation using Ac_2O/pyridine/DMF (1:2:7 v/v/v, 10 mL, 5 min). Non-standard Fmoc-L-Lys(Alloc)-OH was used to introduce the Alloc-protected lysine and Boc-L-Cys(Trt)-OH was used as the N-terminal amino acid. Removal of the N-Alloc protecting group of the Lys(Alloc) was performed by adding a solution of $Pd(PPh_3)_4$ (0.05 mmol, 0.5 eq., 58 mg) and phenylsilane (2.5 mmol, 25 eq., 0.3 mL) in degassed anhydrous DCM (15 mL) for 1h in the dark (twice).[8] The resin was then washed successively with DCM (2×2 min), DMF (2×2 min), 1% H_2O in DMF (2×2 min), DMF (2×2 min), 1% DIEA in DMF (2×2 min), DMF (2×2 min), sodium diethyldithiocarbamate in DMF (0.12 M, 2×5 min) and DMF (2×2 min). DOTA-tris(*t*Bu)ester (0.2 mmol, 114 mg, 2 eq.) was dissolved in a small amount of DMF and added to the resin, then a solution of PyBOP (0.2 mmol, 104 mg, 2 eq.) and DIEA (0.6 mmol, 104 µL, 6 eq) in DMF (2 mL) was added. The resin was agitated overnight at room temperature and the coupling step was repeated once for 4h. The resin was washed with DMF (2×2 min), DCM (2×2 min) and Et_2O (2×2 min) and dried. Removal of acid-labile side chain protecting groups and cleavage were performed using TFA/H_2O/TIS/thioanisole (92.5:2.5:2.5:2.5 v/v/v/v, 10 mL) for 4 h. The peptide was precipitated in cold Et_2O/heptane (1:1 v/v, 150 mL), centrifuged, dissolved in deionized water, lyophilized and purified by HPLC to give 2b (57 mg, 21% yield for the 2b·$(TFA)_8$ salt, 0.1 mmol scale). HPLC (anal.): t_R = 5.4 min (method A); LRMS (ESI+): average *m/z* = 1343.3 (2+), 895.9 (3+), 672.3 (4+), 538.0 (5+), 448.5 (6+) / calculated av. *m/z* = 1343.54 $[M+2H]^{2+}$, 896.03 $[M+3H]^{3+}$, 672.28 $[M+4H]^{4+}$, 538.02 $[M+5H]^{5+}$, 448.52 $[M+6H]^{6+}$ for M = $C_{116}H_{194}N_{36}O_{35}S$); deconvoluted mass found = 2684.6 / expected mass = 2685.07 (average isotopic composition).

Formation of Ln^{3+} complexes $2b^{Ln}$ (Ln = Tb, Eu, Nd or Yb): Metalation of **2b** with Ln^{3+} was performed as described above for $\mathbf{1b^{Ln|Cs124}}$, but under argon to minimize disulfide formation. Nevertheless, before HPLC purification, TCEP (35 µmol, 10 mg) was added to the solution, the pH was adjusted to 6 and the solution was stirred for 30 min to reduce potential disulfide.

$2b^{Tb}$: HPLC (anal.): t_R = 5.4 min (method A); LRMS (ESI+): average *m/z* = 1421.0 (2+), 947.9 (3+), 711.2 (4+), 569.3 (5+), 474.5 (6+) / calculated av. *m/z* = 1421.50 $[M+2H]^{2+}$, 948.00 $[M+3H]^{3+}$, 711.25 $[M+4H]^{4+}$, 569.20 $[M+5H]^{5+}$, 474.50 $[M+6H]^{6+}$ for M = $C_{116}H_{191}N_{36}O_{35}STb$); deconvoluted mass found = 2841.0 / expected mass = 2840.98 (average isotopic composition).

$2b^{Eu}$: HPLC (anal.): t_R = 5.4 min (method A); LRMS (ESI+): average *m/z* = 1417.7 (2+), 945.8 (3+), 709.6 (4+), 567.9 (5+) / calculated av. *m/z* = 1418.01 $[M+2H]^{2+}$, 945.68 $[M+3H]^{3+}$, 709.51 $[M+4H]^{4+}$, 567.81 $[M+5H]^{5+}$ for M = $C_{116}H_{191}N_{36}O_{35}SEu$); deconvoluted mass found = 2834.4 / expected mass = 2834.01 (average isotopic composition).

$2b^{Nd}$: HPLC (anal.): t_R = 5.9 min (method A); LRMS (ESI+): average *m/z* = 1413.3 (2+), 943.1 (3+), 707.6 (4+), 566.2 (5+), 471.9 (6+) / calculated av. *m/z* = 1414.15 $[M+2H]^{2+}$, 943.10 $[M+3H]^{3+}$, 707.58 $[M+4H]^{4+}$, 566.26 $[M+5H]^{5+}$, 472.06 $[M+6H]^{6+}$ for M = $C_{116}H_{191}N_{36}O_{35}SNd$); deconvoluted mass found = 2825.6 / expected mass = 2826.29 (average isotopic composition).

$2b^{Yb}$: HPLC (anal.): t_R = 5.9 min (method A); LRMS (ESI+): average *m/z* = 1428.2 (2+), 952.5 (3+), 714.8 (4+), 571.9 (5+) / calculated av. *m/z* = 1428.55 $[M+2H]^{2+}$, 952.70 $[M+3H]^{3+}$, 714.78 $[M+4H]^{4+}$, 572.02 $[M+5H]^{5+}$ for M = $C_{116}H_{191}N_{36}O_{35}SYb$); deconvoluted mass found = 2855.2 / expected mass = 2855.08 (average isotopic composition).

Preparation of r-LZF and LZF probes by native chemical ligation of segments 1 and 2: A TCEP/MPAA solution was prepared by dissolving TCEP (28.7 mg, 0.1 mmol) and MPAA (16.8 mg, 0.1 mmol) in 0.1 M pH 7.5 sodium phosphate buffer (1 mL). The pH of the solution was adjusted to 6.5 using aq. NaOH (2 M). Peptides **1** (0.5-1.0 µmol) and **2** (1.1 eq.) were dissolved in the TCEP/MPAA solution (140-280 µL, final peptide concentration 3.5 mM, pH 6.5). The native chemical ligation was performed at 37°C and monitored by HPLC. At the end (*ca.* 18-24 h), the reaction

mixture was diluted with 5 % aq. TFA (2 mL), MPAA was extracted by Et_2O. The peptide was purified by HPLC. For ligations with **1a**^{DMN} and **1a**^{AAQ}, DTT was used as a reducing agent instead of TCEP.

r-LZF1$^{Eu|Cs124|Tb}$: Isolated yield = 25%; HPLC (anal.): t_R = 6.9 min (method A); LRMS (ESI+): average *m/z* = 1508.3 (3+), 1131.3 (4+), 905.4 (5+), 754.8 (6+), 647.1 (7+), 566.4 (8+) / calculated av. *m/z* = 1508.20 $[M+3H]^{3+}$, 1131.40 $[M+4H]^{4+}$, 905.32 $[M+5H]^{5+}$, 754.60 $[M+6H]^{6+}$, 646.95 $[M+7H]^{7+}$, 566.20 $[M+8H]^{8+}$ for M = $C_{181}H_{286}N_{54}O_{58}S_2TbEu$; deconvoluted mass found = 4522.2 / expected mass = 4521.57 (average isotopic composition).

r-LZF1$^{Tb|Cs124|Eu}$: Isolated yield = 35%; HPLC (anal.): t_R = 6.9 min (method A); LRMS (ESI+): average *m/z* = 1507.9 (3+), 1131.3 (4+), 905.3 (5+), 754.8 (6+), 647.1 (7+), 566.3 (8+) / calculated av. *m/z* = 1508.20 $[M+3H]^{3+}$, 1131.40 $[M+4H]^{4+}$, 905.32 $[M+5H]^{5+}$, 754.60 $[M+6H]^{6+}$, 646.95 $[M+7H]^{7+}$, 566.20 $[M+8H]^{8+}$ for M = $C_{181}H_{286}N_{54}O_{58}S_2TbEu$; deconvoluted mass found = 4522.2 / expected mass = 4521.57 (average isotopic composition).

LZF3$^{Cs124|Tb}$: Isolated yield = 15%; HPLC (anal.): t_R = 7.1 min (method A); LRMS (ESI+): average *m/z* = 1357.5 (3+), 1018.5 (4+), 815.1 (5+), 679.4 (6+), 582.5 (7+), 509.8 (8+) / calculated av. *m/z* = 1357.78 $[M+3H]^{3+}$, 1018.59 $[M+4H]^{4+}$, 815.08 $[M+5H]^{5+}$, 679.40 $[M+6H]^{6+}$, 582.48 $[M+7H]^{7+}$, 509.80 $[M+8H]^{8+}$ for M = $C_{170}H_{271}N_{50}O_{52}S_2Tb$; deconvoluted mass found = 4070.4 / expected mass = 4070.34 (average isotopic composition).

LZF3$^{Cs124|Eu}$: Isolated yield = 16%; HPLC (anal.): t_R = 7.1 min (method A); LRMS (ESI+): average *m/z* = 1355.4 (3+), 1016.8 (4+), 813.8 (5+), 678.3 (6+), 581.6 (7+), 509.0 (8+) / calculated av. *m/z* = 1355.47 $[M+3H]^{3+}$, 1016.85 $[M+4H]^{4+}$, 813.68 $[M+5H]^{5+}$, 678.23 $[M+6H]^{6+}$, 581.49 $[M+7H]^{7+}$, 508.93 $[M+8H]^{8+}$ for M = $C_{170}H_{271}N_{50}O_{52}S_2Eu$; deconvoluted mass found = 4063.8 / expected mass = 4063.38 (average isotopic composition).

LZF1$^{DPP|Nd}$: Isolated yield = 19%; HPLC (anal.): t_R = 7.5 min (method A); LRMS (ESI+): average *m/z* = 1444.8 (3+), 1083.5 (4+), 867.0 (5+), 722.9 (6+) / calculated av. *m/z* = 1444.63 $[M+3H]^{3+}$, 1083.72 $[M+4H]^{4+}$, 867.18 $[M+5H]^{5+}$, 722.82 $[M+6H]^{6+}$ for M = $C_{177}H_{272}N_{51}O_{59}S_4Nd$; deconvoluted mass found = 4329.4 / expected mass = 4330.87 (average isotopic composition).

LZF1$^{DPP|Yb}$: Isolated yield = 21%; HPLC (anal.): t_R = 5.0 min (method B); ESI-MS average *m/z* = 1454.0 (3+), 1090.8 (4+), 872.9 (5+), 727.7 (6+) / calculated av. *m/z* = 1454.23 $[M+3H]^{3+}$, 1090.93 $[M+4H]^{4+}$, 872.94 $[M+5H]^{5+}$, 727.62 $[M+6H]^{6+}$ for M = $C_{177}H_{272}N_{51}O_{59}S_4Yb$; deconvoluted mass found = 4359.2 / expected mass = 4359.67 (average isotopic composition).

LZF1$^{AAQ|Nd}$: Isolated yield = 27%; HPLC (anal.): t_R = 8.7 min (method A); LRMS (ESI+): average *m/z* = 1321.2 (3+), 991.3 (4+), 793.4 (5+), 661.3 (6+), 567.0 (7+), 496.3 (8+) / calculated av. *m/z* = 1322.18 $[M+3H]^{3+}$, 991.88 $[M+4H]^{4+}$, 793.71 $[M+5H]^{5+}$, 651.59 $[M+6H]^{6+}$, 567.22 $[M+7H]^{7+}$, 496.45 $[M+8H]^{8+}$ for M = $C_{167}H_{259}N_{48}O_{51}S_2Nd$; deconvoluted mass found = 3961.4 / expected mass = 3963.51 (average isotopic composition).

LZF1$^{AAQ|Yb}$: Isolated yield = 24%; HPLC (anal.): t_R = 8.8 min (method A); ESI-MS average *m/z* = 1331.5 (3+), 998.8 (4+), 799.3 (5+), 666.3 (6+), 571.3 (7+), 500.0 (8+) / calculated av. *m/z* = 1331.78 $[M+3H]^{3+}$, 999.09 $[M+4H]^{4+}$, 799.47 $[M+5H]^{5+}$, 666.39 $[M+6H]^{6+}$, 571.34 $[M+7H]^{7+}$, 500.05 $[M+8H]^{8+}$ for M = $C_{167}H_{259}N_{48}O_{51}S_2Yb$; deconvoluted mass found = 3991.6 / expected mass = 3992.31 (average isotopic composition).

LZF3$^{DEAC|Nd}$: Isolated yield = 32%; HPLC (anal.): t_R = 8.4 min (method A); LRMS (ESI+): average *m/z* = 1348.1 (3+), 1011.6 (4+), 809.5 (5+), 674.8 (6+), 578.6 (7+), 506.4 (8+) / calculated av. *m/z* = 1348.56 $[M+3H]^{3+}$, 1011.67 $[M+4H]^{4+}$, 809.54 $[M+5H]^{5+}$, 674.78 $[M+6H]^{6+}$, 578.53 $[M+7H]^{7+}$, 506.34 $[M+8H]^{8+}$ for M = $C_{170}H_{272}N_{49}O_{52}S_2Nd$; deconvoluted mass found = 4042.8 / expected mass = 4042.65 (average isotopic composition).

LZF3$^{DEAC|Yb}$: Isolated yield = 23%; HPLC (anal.): t_R = 8.4 min (method A); ESI-MS average *m/z* = 1358.3 (3+), 1018.8 (4+), 815.5 (5+), 679.8 (6+), 582.8 (7+), 510.2 (8+) / calculated av. *m/z* = 1358.16 $[M+3H]^{3+}$, 1018.87 $[M+4H]^{4+}$, 815.30 $[M+5H]^{5+}$, 679.58 $[M+6H]^{6+}$, 582.64 $[M+7H]^{7+}$, 509.94 $[M+8H]^{8+}$ for M = $C_{170}H_{272}N_{49}O_{52}S_2Yb$; deconvoluted mass found = 4072.7 / expected mass = 4071.45 (average isotopic composition).

LZF3$^{DMN|Nd}$: Isolated yield = 44%; HPLC (anal.): t_R = 5.3 min (method B); LRMS (ESI+): average *m/z* = 1341.7 (3+), 1006.5 (4+), 805.3 (5+), 671.2 (6+), 575.8 (7+) / calculated av. *m/z* = 1341.88 $[M+3H]^{3+}$, 1006.66 $[M+4H]^{4+}$, 805.53 $[M+5H]^{5+}$, 671.44 $[M+6H]^{6+}$, 575.67 $[M+7H]^{7+}$ or M = $C_{170}H_{268}N_{49}O_{51}S_2Nd$; deconvoluted mass found = 4021.7 / expected mass = 4022.62 (average isotopic composition).

LZF3$^{DMN|Yb}$: Isolated yield = 28%; HPLC (anal.): t_R = 5.4 min (method B); ESI-MS average *m/z* = 1351.0 (3+), 1013.6 (4+), 810.9 (5+), 675.9 (6+), 579.6 (7+) / calculated av. *m/z* = 1351.48 $[M+3H]^{3+}$, 1013.86 $[M+4H]^{4+}$, 811.29 $[M+5H]^{5+}$, 676.24 $[M+6H]^{6+}$, 579.78 $[M+7H]^{7+}$ for M = $C_{170}H_{268}N_{49}O_{51}S_2Yb$; deconvoluted mass found = 4050.3 / expected mass = 4051.42 (average isotopic composition).

LZF3$^{Anthra|Nd}$: Isolated yield = 51%; HPLC (anal.): t_R = 8.9 min (method A); LRMS (ESI+): average *m/z* = 1339.8 (3+), 1005.2 (4+), 804.4 (5+), 670.6 (6+), 574.9 (7+) / calculated av. *m/z* = 1340.22 $[M+3H]^{3+}$, 1005.42 $[M+4H]^{4+}$, 804.54 $[M+5H]^{5+}$, 670.61 $[M+6H]^{6+}$, 574.96 $[M+7H]^{7+}$ for M = $C_{172}H_{269}N_{48}O_{50}S_2Nd$; deconvoluted mass found = 4016.7 / expected mass = 4017.64 (average isotopic composition).

LZF3$^{Anthra|Yb}$: Isolated yield = 50%; HPLC (anal.): t_R = 8.8 min (method A); LRMS (ESI+): average *m/z* = 1349.3 (3+), 1012.6 (4+), 810.3 (5+), 675.6 (6+), 579.2 (7+) / calculated av. *m/z* = 1349.82 $[M+3H]^{3+}$, 1012.62 $[M+4H]^{4+}$, 810.30 $[M+5H]^{5+}$, 675.42 $[M+6H]^{6+}$, 579.07 $[M+7H]^{7+}$ for M = $C_{172}H_{269}N_{48}O_{50}S_2Yb$; deconvoluted mass found = 4046.4 / expected mass = 4046.45 (average isotopic composition).

r-LZF3$^{Yb|Anthra|Nd}$: Isolated yield = 60%; HPLC (anal.): t_R = 9.9 min (method A); LRMS (ESI+): average *m/z* = 1511.4 (3+), 1133.8 (4+), 907.3 (5+), 756.4 (6+), 648.4 (7+) / calculated av. *m/z* = 1511.68 $[M+3H]^{3+}$, 1134.01 $[M+4H]^{4+}$, 907.41 $[M+5H]^{5+}$, 756.34 $[M+6H]^{6+}$, 648.44 $[M+7H]^{7+}$, 567.51 $[M+8H]^{8+}$ for M = $C_{186}H_{290}N_{52}O_{56}S_2NdYb$; deconvoluted mass found = 4531.6 / expected mass = 4532.02 (average isotopic composition).

r-LZF3$^{Nd|Anthra|Yb}$: Isolated yield = 56%; HPLC (anal.): t_R = 9.5 min (method A); LRMS (ESI+): average *m/z* = 1511.3 (3+), 1133.9 (4+), 907.4 (5+), 756.3 (6+), 648.4 (7+), 567.5 (8+) / calculated av. *m/z* = 1511.68 $[M+3H]^{3+}$, 1134.01 $[M+4H]^{4+}$, 907.41 $[M+5H]^{5+}$, 756.34 $[M+6H]^{6+}$, 648.44 $[M+7H]^{7+}$, 567.51 $[M+8H]^{8+}$ for M = $C_{186}H_{290}N_{52}O_{56}S_2NdYb$; deconvoluted mass found = 4531.2 / expected mass = 4532.02 (average isotopic composition).

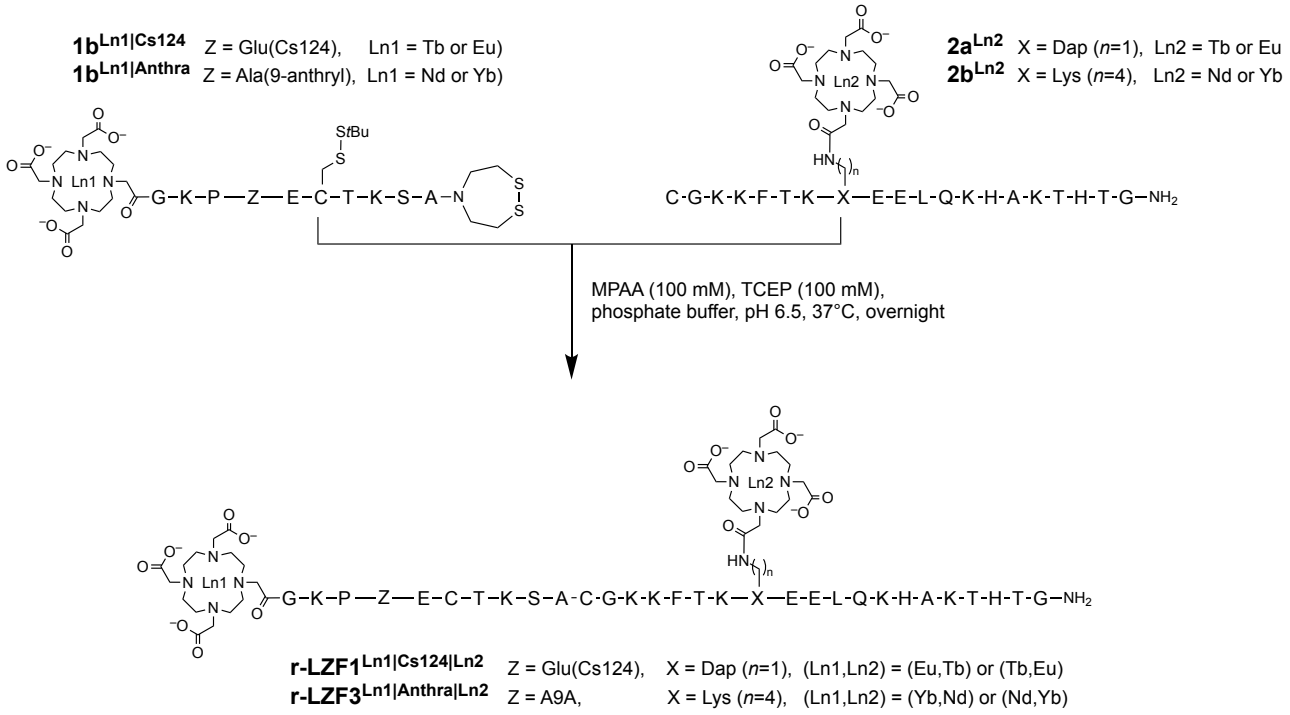

Figure S6. Preparation of hetero-bis-lanthanide probes by NCL. A9A denotes 3-(9-anthryl)-L-alanine.

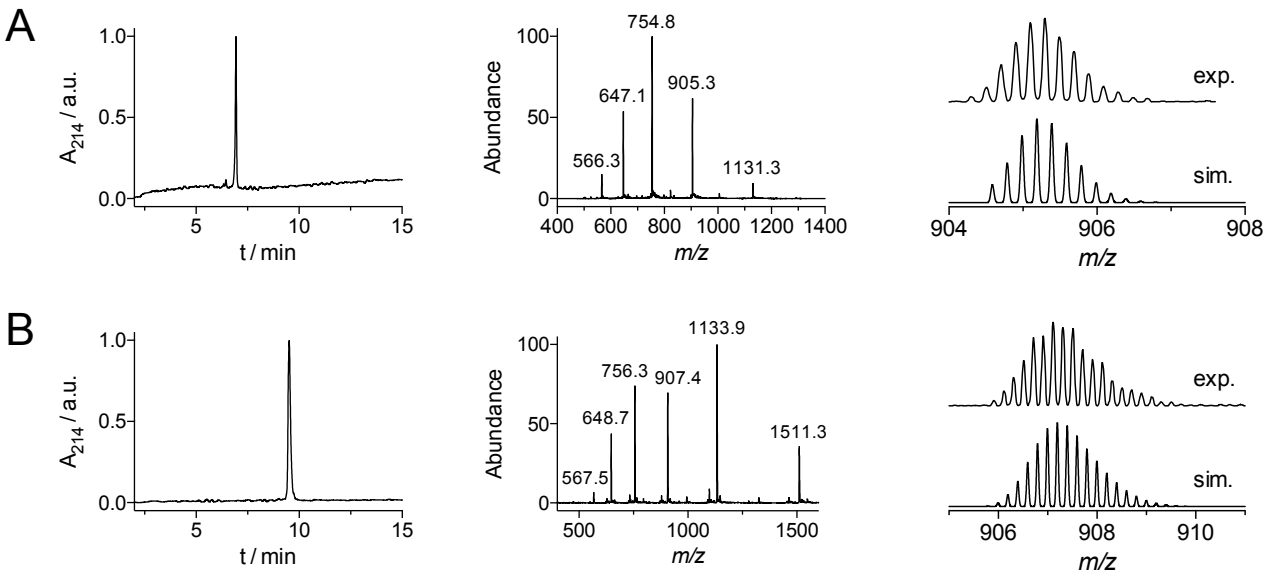

Figure S7. Typical examples of HPLC chromatograms (*left*) and ESI-MS spectra (*middle*: full MS spectrum; *right*: experimental and simulated isotopic pattern of the $[M+5H]^{5+}$ peak) obtained for the above compounds. (A) **r-LZF1**$^{\mathbf{Tb|Cs124|Eu}}$ and (B) **r-LZF3**$^{\mathbf{Nd|Anthra|Yb}}$.

ESI-MS monitoring of the absence of Ln^{3+} scrambling

A solution of $2a^{Eu}$ (0.4 mg) in NH_4OAc buffer (0.1 M, pH 6.9, 200 µL) was prepared and let under air to convert $2a^{Eu}$ into its dimeric disulphide form, in order to prevent the N-terminal cysteine to react with $1b^{Tb|Cs24}$. Then $1b^{Tb|Cs24}$ (0.2 mg) was added to the solution. Half of the solution was analysed immediately while the other half was stirred at room temperature for 72 h. Formation of $1b^{Eu|Cs124}$ and $2a^{Tb}$ was not observed after 72 h.

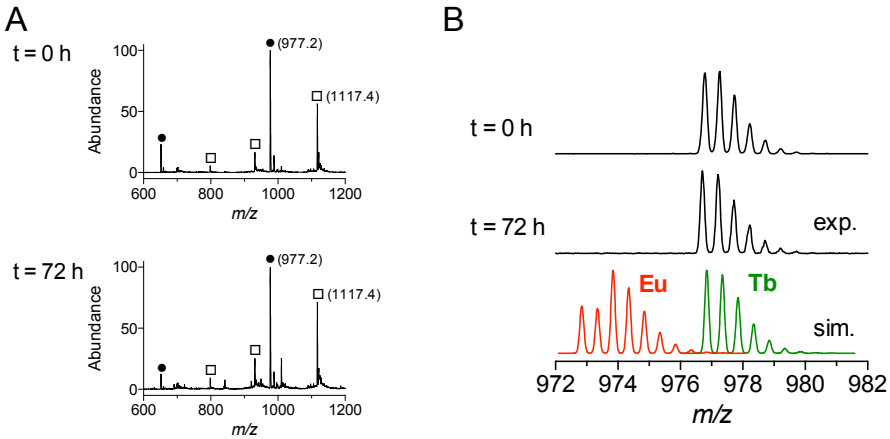

Figure S8. (A) ESI-MS spectra of the mixture of peptides $\mathbf{1b}^{\mathbf{Tb|Cs124}}$ (●) and $\mathbf{2a}^{\mathbf{Eu}}$ (dimeric disulphide form, □) recorded immediately (top) and 72 h after preparation of the solution. (B) Experimental isotopic pattern of the $[M+2H]^{2+}$ peak (av. *m/z* = 977.2) of segment $1b^{Tb|Cs124}$ recorded immediately after mixing of peptides $\mathbf{1b}^{\mathbf{Tb|Cs124}}$ and $\mathbf{2a}^{\mathbf{Eu}}$ (top) and 72 h later (middle). The simulated isotopic patterns for $\mathbf{1b}^{\mathbf{Tb|Cs124}}$ (green) and $\mathbf{1b}^{\mathbf{Eu|Cs124}}$ (red) are displayed at the bottom.

Luminescence spectroscopy

Measurements: For Tb^{3+}- and Eu^{3+}-containing samples, emission and excitation spectra were measured on a Varian Cary Eclipse spectrometer equipped with a thermo-regulated (298 K) cell holder or on a modular Fluorolog FL3-22 spectrometer from Horiba-Jobin Yvon-Spex equipped with a double-grating excitation monochromator and an iHR320 imaging spectrometer coupled to an R928P Hamamatsu photomultiplier. Spectra are corrected for wavelength-dependant

spectrometer response. Time-gated Tb^{3+} and Eu^{3+} luminescence spectra were acquired with 100 µs time delay. Tb^{3+} and Eu^{3+} luminescence lifetimes were measured using a Varian Cary Eclipse spectrometer. Quantum yields of europium emission of LZF probes were determined using the Fluorolog spectrometer by a relative method with quinine sulphate in 0.5 M H_2SO_4 as standard.[9] Estimated experimental error for the quantum yield determination is *ca.* 10 %.

For Yb^{3+} and Nd^{3+}-containing samples: Emission and excitation spectra were measured on a custom-designed Horiba Scientific Fluorolog 3 spectrofluorimeter equipped with either a visible photomultiplier tube (PMT) (220–850 nm, R928P; Hamamatsu) or a NIR PMT (940–1650 nm, H10330-75; Hamamatsu) or 300-1400 nm, R5509; Hamamatsu). Excitation and emission spectra were corrected for the instrumental functions. Luminescence lifetimes were determined under an excitation at 355 nm provided by a Nd:YAG laser (YG 980; Quantel). Signals were detected in the NIR by a Hamamatsu H10330-75 PMT. Output signals from the detector were fed into a 500 MHz bandpass digital oscilloscope (TDS 754C; Tektronix), transferred to a PC for data processing with the program Origin 8®. Luminescence lifetimes are averages of at least three independent measurements. Quantum yields were determined with the Fluorolog 3 spectrofluorimeter based on an absolute method using an integration sphere (Model G8, GMP SA, Renens, Switzerland).[10] Each sample was measured several times under comparable experimental conditions. Estimated experimental error for the quantum yield determination is *ca.* 10 %.

Sample preparation and Zn^{2+} titrations: All samples were prepared in a HEPES buffer (10 mM, pH 7.5) containing TCEP or DTT as reducing agent (250 µM). Zn^{2+} titrations were performed using a $Zn(ClO_4)_2$ solution (1.00 mM in H_2O).

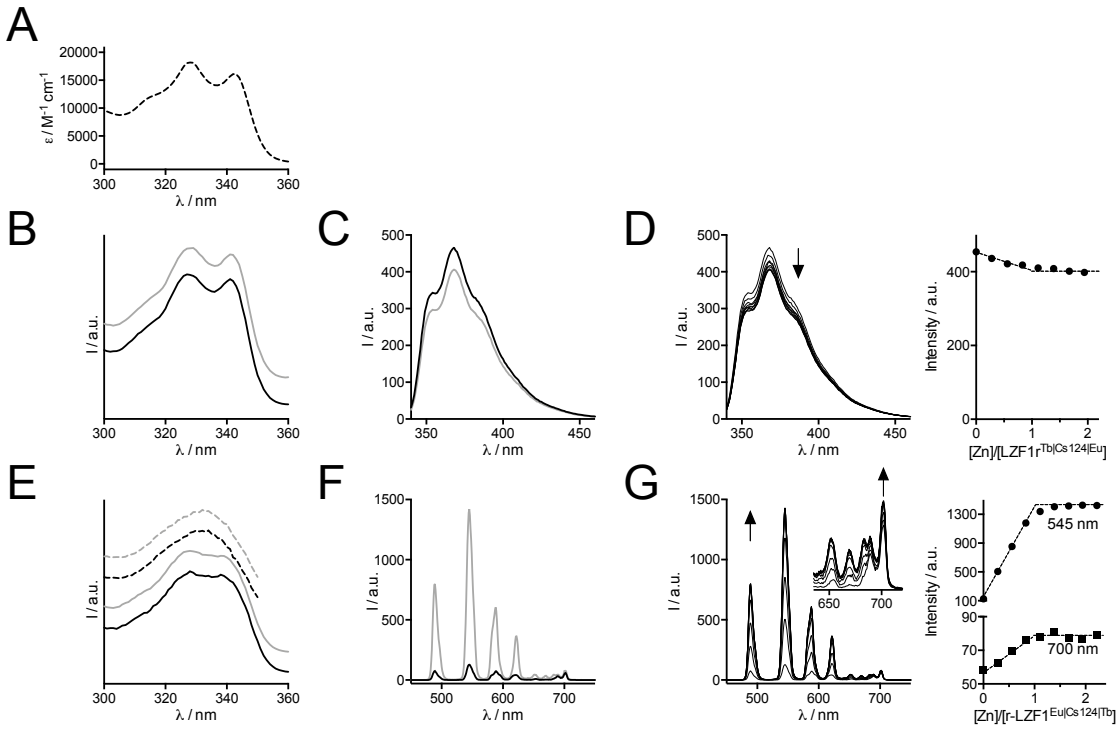

Figure S9. Spectroscopic characterizations of **r-LZF1$^{Eu|Cs124|Tb}$** (7 µM) in its Zn-free (black line) and Zn-bound (grey) forms in HEPES buffer pH 7.5. (A) Absorption spectrum. (B) Fluorescence excitation spectra (λ_{em} = 365 nm). (C) Fluorescence emission spectra (λ_{ex} = 330 nm). (E) Zn^{2+} titration monitored using fluorescence emission. (E) Tb^{3+} (solid lines, λ_{em} = 545 nm) and Eu^{3+} (dashed lines, λ_{em} = 700 nm) time-gated luminescence excitation spectra. (F) Time-gated luminescence emission spectra (λ_{ex} = 330 nm). (G) Zn^{2+} titration monitored using time-gated luminescence emission showing, on the right side, the evolution of the emission at 545 nm (Tb^{3+}) and 700 nm (Eu^{3+}).

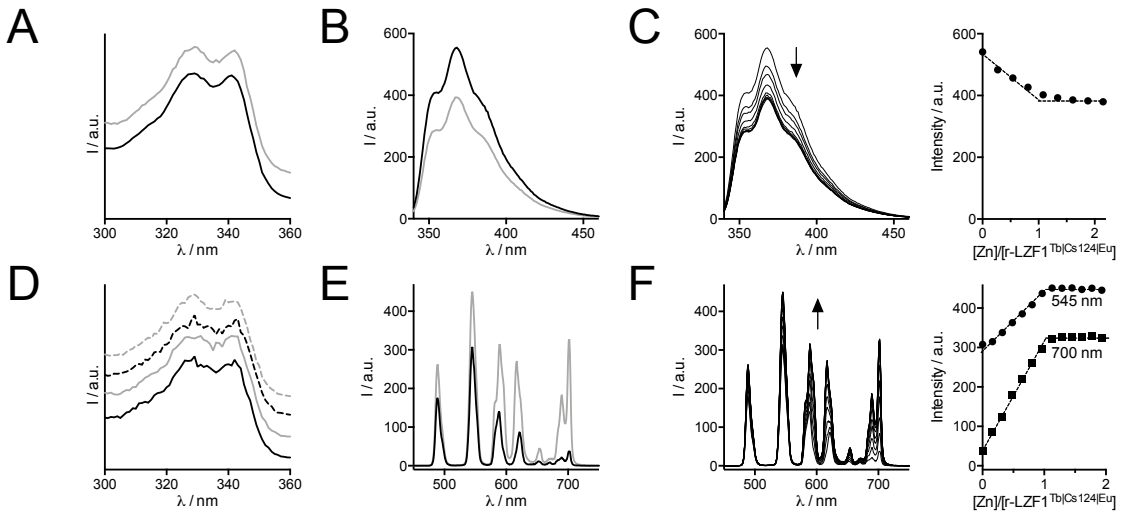

Figure S10. Spectroscopic characterizations of **r-LZF1$^{Tb|Cs124|Eu}$** (7 μM) in its Zn-free (black line) and Zn-bound (grey) forms in HEPES buffer pH 7.5. (A) Absorption spectrum. (B) Fluorescence excitation spectra (λ_{em} = 365 nm). (C) Fluorescence emission spectra (λ_{ex} = 330 nm). (E) Zn^{2+} titration monitored using fluorescence emission. (E) Tb^{3+} (solid lines, λ_{em} = 545 nm) and Eu^{3+} (dashed lines, λ_{em} = 700 nm) time-gated luminescence excitation spectra. (F) Time-gated luminescence emission spectra (λ_{ex} = 330 nm). (G) Zn^{2+} titration monitored using time-gated luminescence emission showing, on the right side, the evolution of the emission at 545 nm (Tb^{3+}) and 700 nm (Eu^{3+}).

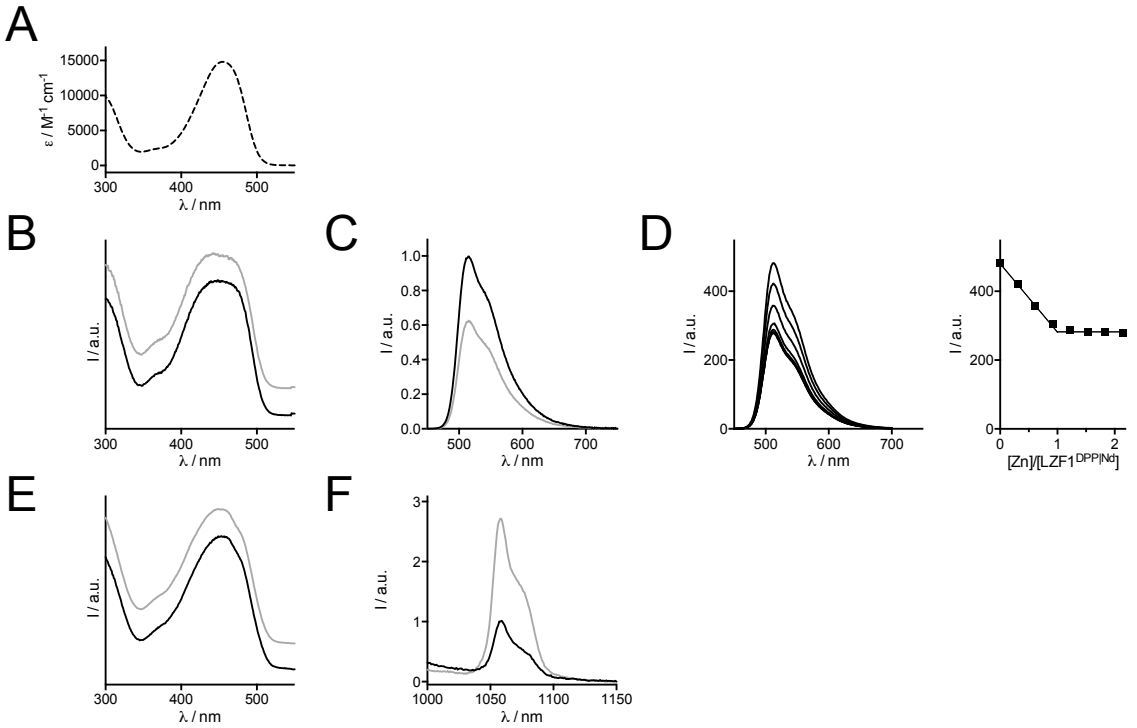

Figure S11. Spectroscopic characterizations of **LZF1$^{DPP|Nd}$** (50 μM) in its Zn-free (black line) and Zn-bound (grey) forms in HEPES buffer pH 7.5. (A) Absorption spectrum. (B) Fluorescence excitation spectra (λ_{em} = 560 nm). (C) Fluorescence emission spectra (λ_{ex} = 440 nm). (D) Zn^{2+} titration monitored using fluorescence emission. (E) Nd^{3+} luminescence excitation spectra (λ_{em} = 1064 nm). (F) Nd^{3+} emission spectra (λ_{ex} = 450 nm).

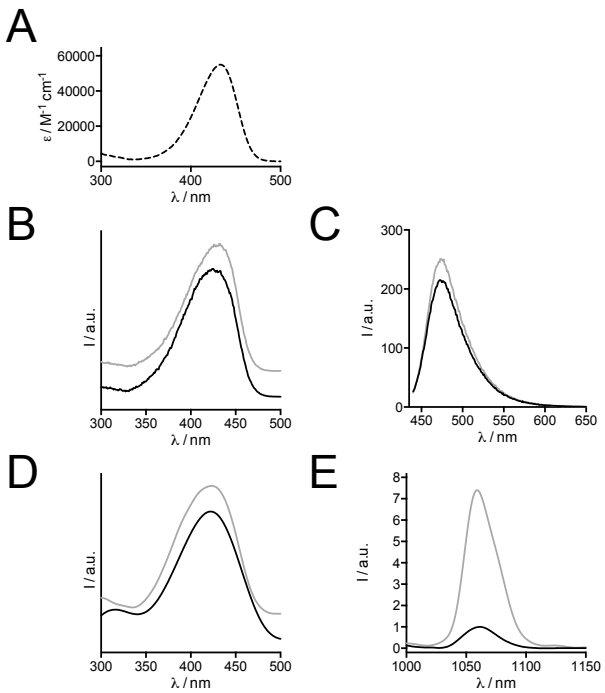

Figure S12. Spectroscopic characterizations of **LZF3$^{DEAC|Nd}$** (50 μM) in its Zn-free (black line) and Zn-bound (grey) forms in HEPES buffer pH 7.5. (A) Absorption spectrum. (B) Fluorescence excitation spectra (λ_{em} = 510 nm). (C) Fluorescence emission spectra (λ_{ex} = 430 nm). (D) Nd^{3+} luminescence excitation spectra (λ_{em} = 1060 nm). (E) Nd^{3+} emission spectra (λ_{ex} = 430 nm).

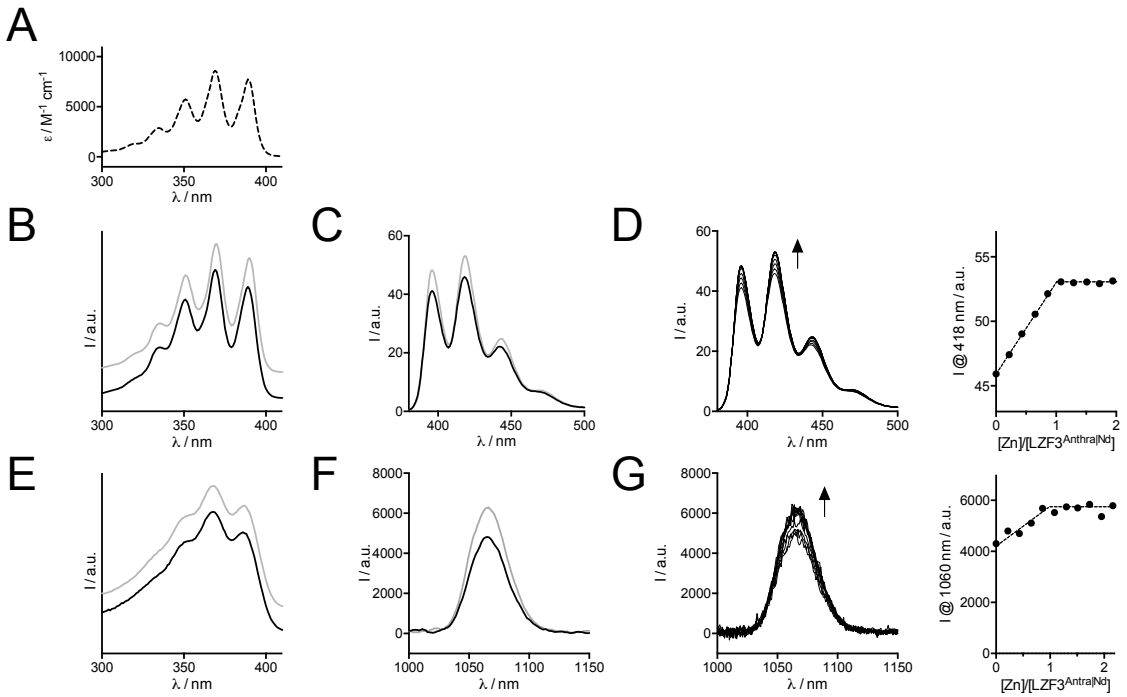

Figure S13. Spectroscopic characterizations of **LZF3$^{Anthra|Nd}$** (50 μM) in its Zn-free (black line) and Zn-bound (grey) forms in HEPES buffer pH 7.5. (A) Absorption spectrum. (B) Fluorescence excitation spectra (λ_{em} = 418 nm). (C) Fluorescence emission spectra (λ_{ex} = 370 nm). (D) Zn^{2+} titration monitored using fluorescence emission. (E) Nd^{3+} luminescence excitation spectra (λ_{em} = 1064 nm). (F) Nd^{3+} emission spectra (λ_{ex} = 370 nm). (G) Zn^{2+} titration monitored using Nd^{3+} luminescence emission.

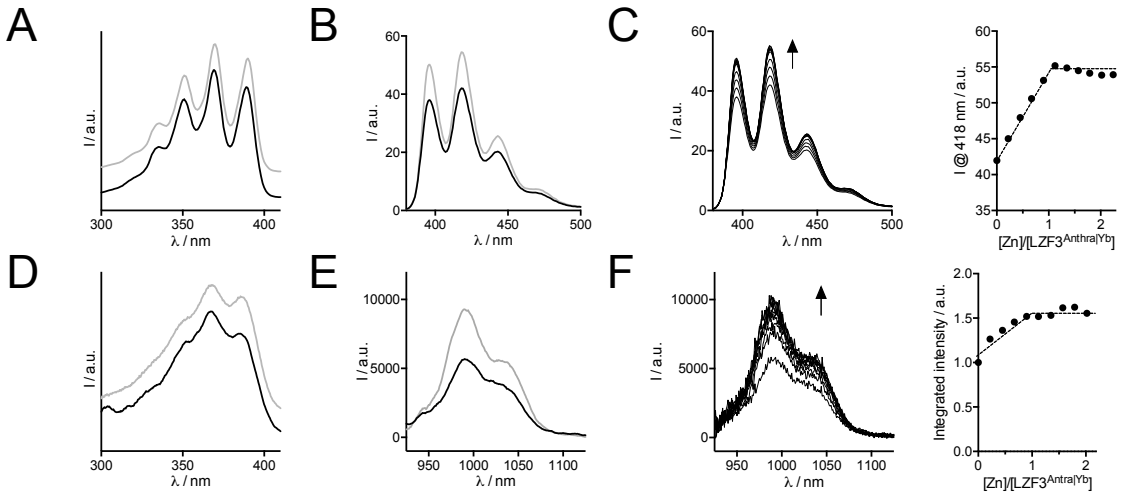

Figure S14. Spectroscopic characterizations of **LZF3$^{\mathbf{Anthra|Yb}}$** (50 μM) in its Zn-free (black line) and Zn-bound (grey) forms in HEPES buffer pH 7.5. (A) Fluorescence excitation spectra (λ_{em} = 418 nm). (C) Fluorescence emission spectra (λ_{ex} = 370 nm). (D) Zn^{2+} titration monitored using fluorescence emission. (E) Yb^{3+} luminescence excitation spectra (λ_{em} = 990 nm). (F) Yb^{3+} emission spectra (λ_{ex} = 370 nm). (G) Zn^{2+} titration monitored using Yb^{3+} luminescence emission.

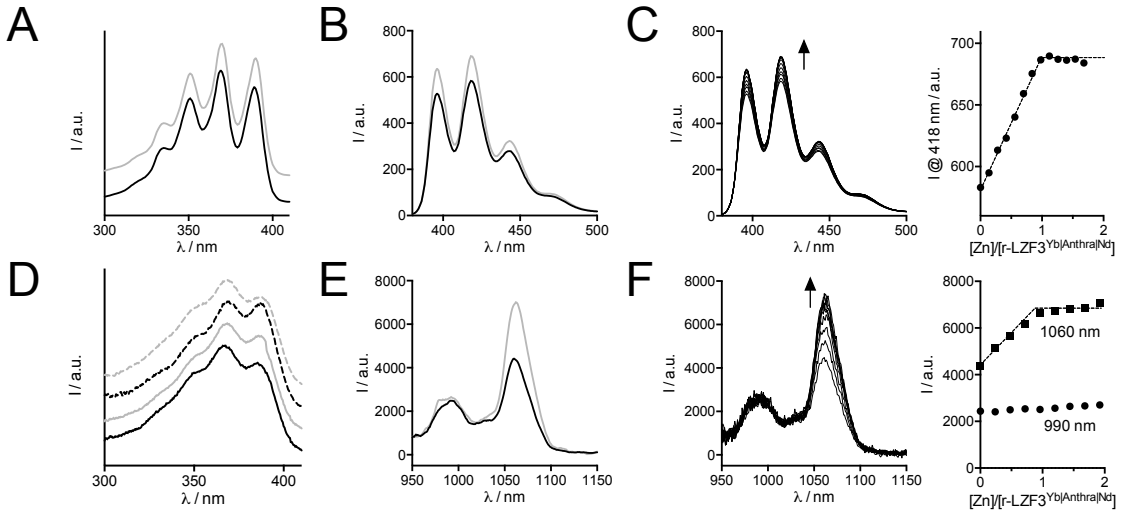

Figure S15. Spectroscopic characterizations of **r-LZF3$^{\mathbf{Yb|Anthra|Nd}}$** (25 μM) in its Zn-free (black line) and Zn-bound (grey) forms in HEPES buffer pH 7.5. (A) Fluorescence excitation spectra (λ_{em} = 418 nm). (B) Fluorescence emission spectra (λ_{ex} = 370 nm). (C) Zn^{2+} titration monitored using fluorescence emission. (D) Yb^{3+} (solid lines, λ_{em} = 990 nm) and Nd^{3+} (dashed lines, λ_{em} = 1060 nm) time-gated luminescence excitation spectra. (E) Lanthanide emission spectra (λ_{ex} = 370 nm). (F) Zn^{2+} titration monitored using lanthanide luminescence emission showing, on the right side, the evolution of the emission at 990 nm (Yb^{3+}) and 1060 nm (Nd^{3+}).

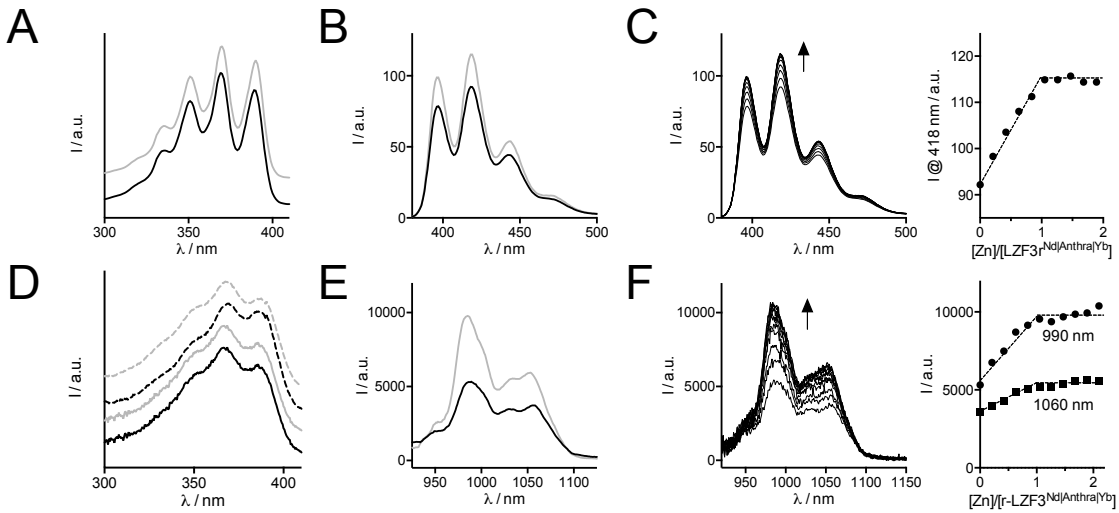

Figure S16. Spectroscopic characterizations of **r-LZF3$^{Nd|Anthra|Yb}$** (25 μM) in its Zn-free (black line) and Zn-bound (grey) forms in HEPES buffer pH 7.5. (A) Fluorescence excitation spectra (λ_{em} = 418 nm). (B) Fluorescence emission spectra (λ_{ex} = 370 nm). (C) Zn^{2+} titration monitored using fluorescence emission. (D) Yb^{3+} (solid lines, λ_{em} = 990 nm) and Nd^{3+} (dashed lines, λ_{em} = 1060 nm) time-gated luminescence excitation spectra. (E) Lanthanide emission spectra (λ_{ex} = 370 nm). (F) Zn^{2+} titration monitored using lanthanide luminescence emission showing, on the right side, the evolution of the emission at 990 nm (Yb^{3+}) and 1060 nm (Nd^{3+}).

Table S1. Lanthanide luminescence quantum yield (Φ^{Ln}) and lifetimes (τ) for Zn-free and Zn-bound NIR-emitting LZF peptides.

Compound		$\Phi^{Ln} \times 10^3$ / %	τ^{Nd} / ns	τ^{Yb} / μs
LZF1$^{DPP|Nd}$	Zn-free	1.21	108	–
	Zn-bound	3.23	97	–
LZF3$^{DEAC|Nd}$	Zn-free	0.133	124	–
	Zn-bound	0.74	93	–
LZF3$^{Anthra|Nd}$	Zn-free	2.2	102	–
	Zn-bound	2.7	97	–
LZF3$^{Anthra|Yb}$	Zn-free	4.2	–	29.2 (91%), 2.8 (9%)
	Zn-bound	6.0	–	22.0 (89%), 2.0 (11%)
r-LZF3$^{Yb|Anthra|Nd}$	Zn-free	3.9	88	19.4 (87%), 1.8 (13%)
	Zn-bound	4.7	96	18.7 (36%), 5.7 (64%)
r-LZF3$^{Nd|Anthra|Yb}$	Zn-free	4.4	99	10.0 (73%), 1.7 (28%)
	Zn-bound	6.6	88	7.2 (85%), 1.2 (15%)

Determination of *q*, the number of water molecules coordinated to Tb^{3+} and Eu^{3+}: Solutions of r-LZF1$^{Tb|Cs124|Eu}$ in a HEPES buffer (10 mM, pH 7.5) containing TCEP (250 μM) were prepared in various H_2O/D_2O mixtures (25, 50, 75 and 100 % H_2O). Lifetimes in 100 % D_2O were extrapolated from the plot of the rate constants of Ln^{3+} luminescence decay ($k_{Ln} = \tau_{Ln}^{-1}$) against the fraction of H_2O in H_2O/D_2O mixtures (Figure S19). The number of coordinated water molecules (q) was determined using $q = 5\times(k_{Tb/H2O} - k_{Tb/D2O} - 0.06)$ for Tb^{3+} and $q = 1.2\times(k_{Eu/H2O} - k_{Eu/D2O} - 0.325)$ for Eu^{3+}.[11]

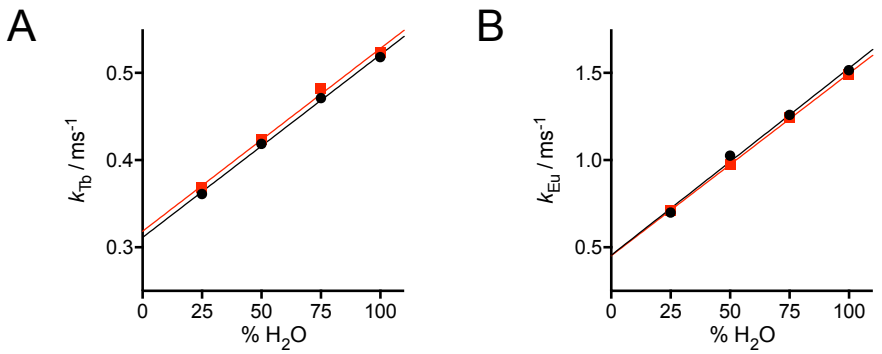

Figure S17. Plot of the Ln^{3+} luminescence decay rate constants k_{Tb} (A) and k_{Eu} (B) against the volume fraction of H_2O in H_2O/D_2O mixtures for free (black) and Zn-bound (red) **r-LZF1$^{Tb|Cs124|Eu}$**. Luminescence decays were recorded in a HEPES buffer (10 mM, pH 7.5).

Table S2. Lanthanide luminescence lifetimes (τ) and hydration numbers (q) for Zn-free and Zn-bound r-LZF1$^{Tb|Cs124|Eu}$.

Compound		Ln^{3+}	τ in H_2O / ms	τ in D_2O / ms	q (± 0.3)
r-LZF1$^{Tb\|Cs124\|Eu}$	Zn-free	Tb^{3+}	1.93 (1)	3.22 (1)	0.7
		Eu^{3+}	0.66 (1)	2.20 (1)	0.9
	Zn-bound	Tb^{3+}	1.91 (1)	3.14 (1)	0.7
		Eu^{3+}	0.67 (1)	2.22 (1)	0.9

Influence of Dap *vs* Lys anchorage for DOTA (LZF1 *vs* LZF3)

The C-terminal segment 2a with Dap anchorage for the DOTA ligand was obtained with a low 8% yield due to uncomplete deprotection of Dap(Alloc) used during the synthesis (see ref. [5]). Repeating Pd^0 treatment several times never allowed to get more than 60% conversion during the Alloc removal step and to increase the yield. On contrary, the use of a Lys(Alloc) residue allowed complete Alloc removal and better overall yield for the synthesis of the C-terminal segment 2b (21%). In order to evaluate the influence of the Dap to Lys substitution, we prepared peptides **LZF3$^{Cs124|Tb}$** and **LZF3$^{Cs124|Eu}$** with a Lys(DOTA-Ln) residue and compared their luminescence properties to that of the previously described **LZF1$^{Cs124|Tb}$** and **LZF1$^{Cs124|Eu}$** probes with a Dap(DOTA-Ln) residue.[5] They behave the same way, the only difference being (i) a slightly higher luminescence increase upon Zn^{2+} binding (a 16-fold versus a 13-fold increase for the Lys derivative **LZF3$^{Cs124|Tb}$** compared to the Dap derivative **LZF1$^{Cs124|Tb}$** and a 12-fold versus a 9.5-fold increase for the Eu derivatives **LZF3$^{Cs124|Eu}$** and **LZF1$^{Cs124|Eu}$**, respectively) and a slightly lower K_d for the lysine derivatives ($10^{-10.3}$ *vs* $10^{-9.1}$). Therefore, lengthening the anchorage of the DOTA moiety from one carbon (Dap) to four (Lys) has minor effect on the probe behaviour but affords better synthesis yield. The antenna screen was processed using either Dap or Lys anchorage for DOTA.

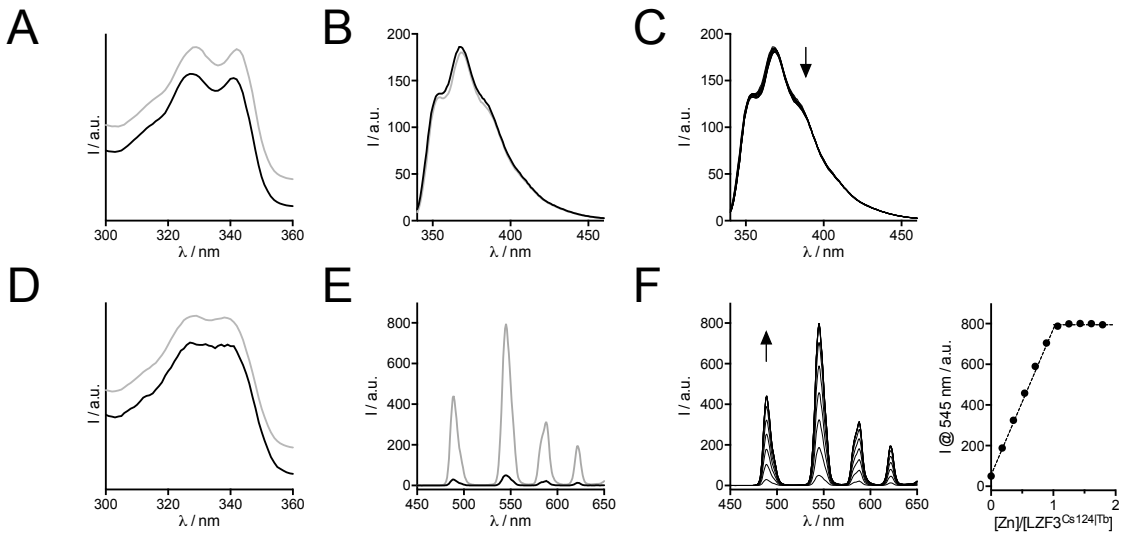

Figure S18. Spectroscopic characterizations of **LZF3$^{Cs124|Tb}$** (10 µm) in its Zn-free (black line) and Zn-bound (grey) forms in HEPES buffer pH 7.5. (A) Fluorescence excitation spectra (λ_{em} = 365 nm). (B) Fluorescence emission spectra (λ_{ex} = 330 nm). (C) Zn^{2+} titration monitored using fluorescence emission. (D) Tb^{3+} time-gated luminescence excitation spectra (λ_{em} = 545 nm). (E) Time-gated luminescence emission spectra (λ_{ex} = 330 nm). (F) Zn^{2+} titration monitored using time-gated luminescence emission.

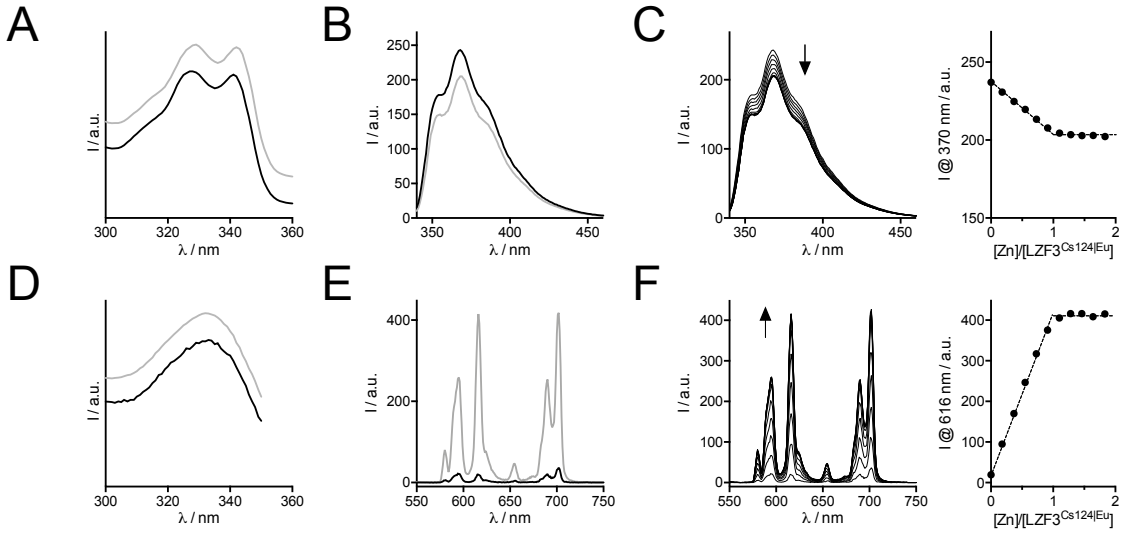

Figure S19. Spectroscopic characterizations of **LZF3$^{Cs124|Eu}$** (10 µm) in its Zn-free (black line) and Zn-bound (grey) forms in HEPES buffer pH 7.5. (A) Fluorescence excitation spectra (λ_{em} = 365 nm). (B) Fluorescence emission spectra (λ_{ex} = 330 nm). (C) Zn^{2+} titration monitored using fluorescence emission. (D) Eu^{3+} time-gated luminescence excitation spectra (λ_{em} = 616 nm). (E) Time-gated luminescence emission spectra (λ_{ex} = 330 nm). (F) Zn^{2+} titration monitored using time-gated luminescence emission.

Determination of Zn^{2+} binding constants

Binding constants were determined by titrating a solution containing the LZF probe and a known amount of an appropriate competitor tested among EDTA, HEDTA and EGTA. For all probes, EDTA and HEDTA were found to be too strong competitors and the binding constants were determined using EGTA. For r-LZF1$^{Tb|Cs124|Eu}$, LZF3$^{Cs124|Tb}$ and LZF3$^{Cs124|Eu}$ time-gated Ln^{3+} emission was used to monitor the titration whereas fluorescence emission was used for r-LZF3$^{Yb|Anthra|Nd}$.

For each titration, the evolution of the intensity against the Zn^{2+}/peptide ratio (r) was fitted to the equilibrium Zn·LZF + EGTA ⇌ LZF + Zn·EGTA by Equations (1-7) in which I_0 and I_F are the emission intensities at the beginning and the end of the titration, $[LZF]_t$, $[EGTA]_t$ and $[Zn]_t$ the total concentrations of LZF, EGTA and Zn^{2+} introduced in the solution. The apparent Zn^{2+} binding constant of EGTA at pH 7.5 was calculated from pK_a and log β_{11} values reported in the literature: $K_{ZnEGTA} = 10^{9.2}$.[12,13] (L The dilution could be neglected. Figure S20 shows the Zn^{2+} titrations of the LZF probes in the presence of EGTA and their fits, which yielded $K_{ZnLZF}/K_{ZnEGTA} = 1.1 \pm 0.1$ (A), 9 ± 1 (B), 8.9 ± 0.5 (C) and 36 ± 8 (B). Table S3 summarizes the binding constants.

$$I = I_0 + \frac{I_F - I_0}{[LZF1]_t} \times \frac{-b - \sqrt{b^2 - 4ac}}{2a} \quad \text{, when } [Zn]_t < [LZF]_t + [EGTA]_t \tag{1}$$

$$I = I_F, \text{ when } [Zn]_t > [LZF]_t + [EGTA]_t \tag{2}$$

$$r = \frac{[Zn]_t}{[LZF]_t} \tag{3}$$

$$a = K - 1 \tag{4}$$

$$b = r[LZF]_t - [EGTA]_t - rK[LZF]_t - K[LZF]_t \tag{5}$$

$$c = rK[LZF]_t^2 \tag{6}$$

$$K = \frac{K_{ZnLZF}}{K_{ZnEGTA}} \tag{7}$$

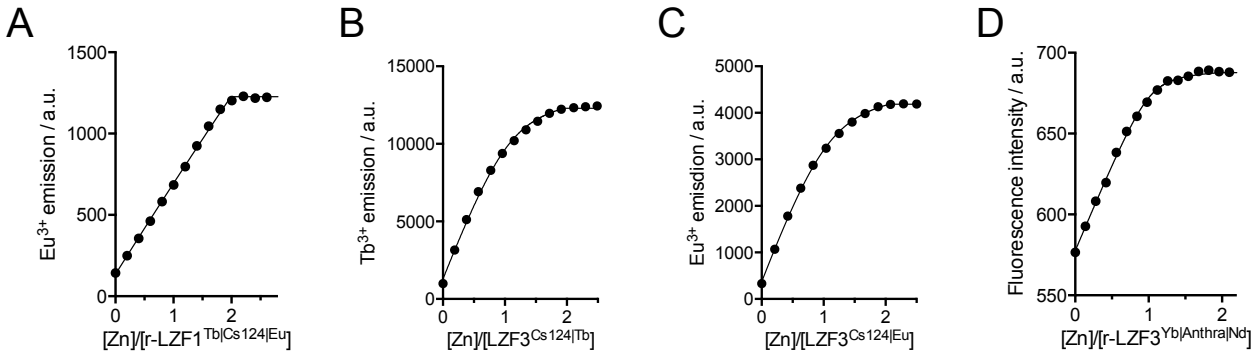

Figure S20. Evolution of (A, B, C) time-gated Ln^{3+} emission or (D) anthracene fluorescence upon addition of Zn^{2+} in a solution of (A) **r-LZF1$^{Tb|Cs124|Eu}$**, (B) **LZF3$^{Cs124|Tb}$**, (C) **LZF3$^{Cs124|Eu}$** and (D) **r-LZF3$^{Yb|Anthra|Nd}$** in a HEPES buffer (10 mM, pH 7.5, 250 µM TCEP) containing EGTA as a competitor. (A) [**r-LZF1$^{Tb|Cs124|Eu}$**] = 10 µM, [EGTA] = 10 µM. (B) [**LZF3$^{Cs124|Tb}$**] = 10 µM, [EGTA] = 10 µM. (C) [**LZF3$^{Cs124|Eu}$**] = 10 µM, [EGTA] = 10 µM. (D) [**r-LZF3$^{Yb|Anthra|Nd}$**] = 12 µM, [EGTA] = 12 µM. The solid lines correspond to the fit to the equilibrium Zn·LZF1 + EGTA ⇌ LZF1 + Zn·EGTA by Equations (1-7).

Table S3. Binding constants.

Compound	log K_{ZnLZF} (or -log K_d)
r-LZF1$^{Tb|Cs124|Eu}$	9.2 ± 0.2
LZF3$^{Cs124|Tb}$	10.2 ± 0.2
LZF3$^{Cs124|Eu}$	10.2 ± 0.2
r-LZF3$^{Yb|Anthra|Nd}$	10.8 ± 0.2

References

[1] A. M. Reynolds, B. R. Sculimbrene, B. Imperiali, *Bioconjugate Chem.* **2008**, *19*, 588–591.
[2] G. Loving, B. Imperiali, *J. Am. Chem. Soc.* **2008**, *130*, 13630–13638.
[3] E. Heyer, P. Lory, J. Leprince, M. Moreau, A. Romieu, M. Guardigli, A. Roda, R. Ziessel, *Angew. Chem., Int. Ed.* **2015**, *54*, 2995–2999.
[4] G. Schwarzenbach, H. Flaschka, *Complexometric Titrations*, Methuen, London, **1969**.
[5] M. Isaac, L. Raibaut, C. Cepeda, A. Roux, D. Boturyn, S. V. Eliseeva, S. Petoud, O. Sénèque, *Chem.-Eur. J.* **2017**, *23*, 10992–10996.
[6] N. Ollivier, L. Raibaut, A. Blanpain, R. Desmet, J. Dheur, R. Mhidia, E. Boll, H. Drobecq, S. L. Pira, O. Melnyk, *J. Pept. Sci.* **2014**, *20*, 92–97.
[7] E. Boll, H. Drobecq, N. Ollivier, A. Blanpain, L. Raibaut, R. Desmet, J. Vicogne, O. Melnyk, *Nat. Protoc.* **2015**, *10*, 269–292.
[8] N. Thieriet, J. Alsina, E. Giralt, F. Guibe, F. Albericio, *Tetrahedron Lett.* **1997**, *38*, 7275–7278.
[9] A. M. Brouwer, *Pure Appl. Chem.* **2011**, *83*, 2213–2228.
[10] H. Ishida, J.-C. Bunzli, A. Beeby, *Pure Appl. Chem.* **2016**, *88*, 701–711.
[11] A. Beeby, I. M. Clarkson, R. S. Dickins, S. Faulkner, D. Parker, L. Royle, A. S. de Sousa, J. A. G. Williams, M. Woods, *J. Chem. Soc., Perkin Trans. 2* **1999**, 493–504.
[12] A. E. Martell, R. M. Smith, *Critical Stability Constants*, Plenum Press, New York, **1974**.
[13] R. M. Smith, A. E. Martell, R. J. Motekaitis, *Critically Selected Stability Constants of Metal Complexes Database. NIST Standard Reference Database 46*, **2001**.